Experimental investigation of the structure of nonionic microemulsions and their relation to the bending elasticity of the amphiphilic film

M. Gradzielski,[1] D. Langevin,[1,*] and B. Farago[2]
[1]*Laboratoire de Physique Statistique, Ecole Normale Superieure, 24 rue Lhomond, F-75231 Paris Cedex 05, France*
[2]*Institut Laue-Langevin, Bôite Postale 156X, F-38042 Grenoble Cedex 9, France*
(Received 2 May 1995)

Oil-in-water microemulsions of nonionic surfactants of type C_nE_j with various hydrocarbons have been characterized by means of small-angle-neutron-scattering (SANS) (carried out at the Laboratoire Leon Brillouin, CEA-CNRS, Saclay, France) and interfacial tension measurements. The obtained structural parameters (radius R and polydispersity index p) of this droplet system and the interfacial tension γ were related to the bending elasticity of the amphiphilic film that can be described by the spontaneous curvature and two elastic constants, bending modulus κ and saddle-splay modulus $\bar{\kappa}$. The validity of our method to extract p from the shape analysis of the scattering curves has been confirmed by an independent contrast variation experiment. Both p and γ lead independently for all systems to very similar values for the elastic moduli. Their sum $2\kappa+\bar{\kappa}$ is proportional to the chain length of the surfactant but independent of our employed hydrocarbons (hexane→decane). Finally, we also performed SANS experiments for a dilution series, where from the concentration dependence of R and p we are able to deduce independently this sum of the elastic constants that agrees well with the values obtained before. The elastic theory of the amphiphilic film allows for a self-consistent interpretation of structural and interfacial tension data and also to reliably predict one of these quantities from the knowledge of the other ones.

PACS number(s): 82.70.Kj

I. INTRODUCTION

Microemulsions are thermodynamically stable systems in which a homogeneous mixture of oil and water is achieved by the stabilizing effect of a surfactant [1–3]. The presence of the surfactant (and cosurfactant and/or electrolyte, respectively) reduces the interfacial tension largely, which allows such a system with a large interface to be stable. The size of their structural units is normally in the range of 30–300 Å, which explains their transparency. For these systems three different structural types have been characterized. They may either contain droplets of oil in water (O-W), droplets of water in oil (W-O), or be made up from a bicontinuous (spongelike) structure [4–6].

The study of microemulsions has generally attracted a lot of interest, and the principles that govern their stability and structure are still the subject of experimental and theoretical investigations. In general the interfacial tension between the microemulsion and the phase to be solubilized is very low. Therefore the gain in dispersion energy is larger than the increase of the interfacial energy. By now it is widely agreed upon that their properties are determined to a large degree by the elastic properties of the amphiphilic film that separates the hydrophobic and hydrophilic regions of the microemulsion [7–13]. Two elastic constants are required to describe the elastic properties of the film: the bending modulus κ and the saddle-splay modulus $\bar{\kappa}$ [7]. However, the determination of these elastic constants is by no means a simple task, and different experimental approaches have been advanced to measure them [14–17]. Yet the different methods do not necessarily yield values that are in agreement. Therefore there seems to remain the necessity to clarify the situation regarding the elastic moduli of amphiphilic films.

Since a knowledge of the elastic constants is an essential requirement for understanding the behavior and properties of microemulsions, we proceeded to study a system that should be as simple as possible and vary in that system systematically molecular parameters (like the chain length of surfactant or oil) in order to see how the molecular structure of the components influences the elastic constants. A particularly suited system for such an investigation should be the microemulsions obtained in the case of the alkyloligoglycolethers C_nE_j. Here one can form a microemulsion without having to resort to introduce a cosurfactant into the system, since, of course, the presence of such an additional component renders the interpretation of its properties more complicated. This means one has the simplest composition possible to form a microemulsion: surfactant, water, and oil.

The nonionic surfactants of type C_nE_j are also insofar interesting, since here all three structural types described above may be attained simply by changing the temperature, i.e., a parameter that can easily be controlled in an experiment [18,19]. Upon increasing the temperature the natural curvature that these systems try to attain will decrease monotonically [20]. At low temperatures the natural curvature c_0 will be positive, and therefore an O-W microemulsion will be formed (it should be noted here that the sign of the curvature is defined in such a way as to be positive if the interface is curved convex toward the

*Present address: Centre de Recherche Paul Pascal, Avenue Docteur Schweitzer, F-33600 Pessac, France.

water). Upon increasing the temperature, c_0 will become close to zero, and in this range bicontinuous systems are observed. Finally at still higher temperatures c_0 will be negative, and here a W-O microemulsion will be stable. This means that with these nonionic surfactants all different structural types of microemulsions can be accomplished within a temperature range of about 15–20 K [19–22], where the precise location of the transition temperature depends on the particular choice of surfactant and hydrocarbon.

All this renders the system C_nE_j-hydrocarbon-water particularly suited for a systematic interpretation of the elastic properties of its amphiphilic film. In the following study we concentrated on O-W droplets, since droplet structures are the simplest structural type and their description in terms of the elastic constants is the furthest advanced [23–28]. To study this system we used small-angle-neutron-scattering (SANS) and interfacial tension measurements. Then we applied theoretical expressions that relate structural properties like particle size and polydispersity, as well as the macroscopical interfacial tension, to the elastic constants in order to calculate values for these constants, which should also show us how well suited the theoretical expressions are to a description of our microemulsions. This has been done for systems where we also systematically varied the chain length of the surfactant as well as of the hydrocarbon, in order to see how their molecular architecture influences the elasticity of the amphiphilic film.

A similar approach has been employed before [29], but with a more limited scope. There mainly the bulk contrast was used in the SANS experiments, whereas here we will exclusively use the shell contrast that should provide much more precise information regarding the polydispersity of the droplets. The results should also be more comparable, since here we employ the same hydrocarbon with surfactants of different chain length, whereas there at the same time the chain length of the hydrocarbon was also varied. In addition in this study we experimentally check the concentration dependence of the droplet structure which is due to the entropy of mixing. By doing so one can verify the theoretical predictions, and obtain an independent estimate of the elastic moduli. Furthermore, this might allow for a judgment about which type of expression has to be used for the entropy of mixing term since there remains still some controversy about that point (see in particular Appendix B). The present study should go well beyond the results of our former investigations [29], and thereby extend the understanding of the corresponding microemulsions significantly.

II. EXPERIMENT

A. Materials

The nonionic surfactants $C_{10}E_4$ [*n*-decyltetra(oxyethylene) ether] and $C_{12}E_5$ [*n*-dodecylpenta (oxyethylene) ether] were obtained from Nikko Chemicals Co. Ltd. (Tokyo, Japan). C_8E_3 [*n*-octyltri(oxyethylene) ether] was purchased from Bachem Feinchemikalien AG (Bubendorf, Switzerland). Decane, octane, heptane, and hexane were obtained from Sigma Chemical Co. (St. Louis) in 99% purity and used as supplied. The deuterated hydrocarbons were all supplied by Euroiso-top Groupe CEA, C.E. Saclay, Gif-sur-Yvette (France). Their isotopic purity was 99% for D_{14}-hexane, D_{18}-octane, and D_{22}-decane. For D_{16}-heptane the isotopic purity was indicated as 98%. D_2O was purchased from the same source, and had an isotopic purity of 99.8%.

For the SANS experiments all samples were prepared by weighing in the appropriate amounts of oil, surfactant, and water. Then they were thermostated at the corresponding experimental temperature for at least 24 h prior to the measurement. Finally they were filled into the sample cells, which were also kept in the thermostat, until they were directly transferred to the thermostated sample rack, in order to ensure that the temperature change during the filling and transfer process was kept at minimum (since as mentioned above the microemulsions are fairly sensitive to temperature changes). If not otherwise indicated, all microemulsion samples were prepared in such a way as to contain a small amount of excess phase in order to ensure two phase equilibrium conditions, i.e., they were saturated with the solubilizate.

In all our data evaluations we used the following scattering length densities: H_2O: -5.60×10^{9} cm^{-2}; D_2O: 6.36×10^{10} cm^{-2}; C_8E_3: 3.14×10^{9} cm^{-2}; $C_{10}E_4$: 2.91×10^{9} cm^{-2}; $C_{12}E_5$: 2.76×10^{9} cm^{-2}; D_{22}-decane: 6.54×10^{10} cm^{-2}; D_{18}-octane: 6.35×10^{10} cm^{-2}; D_{16}-heptane: 6.19×10^{10} cm^{-2}; and D_{14}-hexane: 6.08×10^{10} cm^{-2}.

B. Methods

The small-angle-neutron-scattering (SANS) experiments were carried out at the Laboratoire Léon Brillouin, Saclay (Laboratoire Commune Commissariat à l' Energie Atomique–CNRS). All SANS spectra were recorded at the PAXE instrument. For these measurements the samples were contained in quartz cells (Hellma) of 2-mm thickness and 1-cm width. These cells were placed in a thermostated rack where the samples were thermostated within an accuracy of 0.2 K. The rack can hold up to eight cells, and was closed to the outside, which means that the cells themselves could remain in a dry nitrogen atmosphere in order to avoid water condensation onto the cells during the measurements at low temperatures. The wavelength was always chosen to be 6 Å, and the sample-to-detector distance was 1.57, 3.07, or 5.07 m, thereby covering an effective q range of 0.035–0.23, 0.015–0.12, and 0.008–0.075 1/Å, respectively.

The scattering intensity was detected two dimensionally, and afterwards radially averaged, normalized with respect to the monitor value, and corrected for the efficiency of the individual detector cells (by dividing by a measurement of H_2O that should give a constant scattering intensity since it is an isotropic scatterer), and finally the sample transmission was taken into account. These relative intensity curves were then converted into absolute units (differential scattering cross section in 1/cm) by determination of the intensity of the primary beam with the help of an attenuator, and measuring its attenuation

factor as described in the literature [30]. Finally from all these files the corresponding solvent background, that always had been measured under identical conditions, was subtracted. This is particularly important at the highest sample-to-detector distance, since here this background is no longer a constant as the background scattering (that one already observes upon having the empty quartz cells in the beam) increases toward the low-q region. Files for the same samples at different sample-to-detector distance were then superimposed. This was very possible for all investigated samples, and they never differed by more than 6% with respect to their absolute scale.

The measurements of the interfacial tension were done by the technique of surface laser light scattering; the details of this method have been described before [31]. In this experiment the light impinging on the interface microemulsion/excess phase (which was placed in a thermostated cell) is scattered by thermal fluctuations of this interface. The scattered light intensity is detected by a photomultiplier, analyzed by means of a digital correlator, and then Fourier transformed in order to obtain the frequency spectrum. This spectrum was then fitted with the corresponding theoretical expressions [31] (that depend on viscosities and densities of the two phases) in order to obtain the interfacial tension value.

III. THEORETICAL PART

A. Theory for microemulsions

A typical criterion for the formation of a microemulsion is that the corresponding system will always possess a low interfacial tension γ between the solvent phase and the dispersed excess phase. Typically these values are in the range of $0.1-10^{-3}$ mN/m or even lower. There exist numerous studies that deal with the thermodynamical stability and the structure of microemulsions, starting with the original proposition of Schulmann [32,33] that they possess zero or negative interfacial tension. Meanwhile most current theories concentrate on the bending elasticity of the amphiphilic film as the key factor to explain microemulsion structure [7–13].

In particular, droplet-type structures have been treated in much detail [23–28], and this will concern us since all our experiments were performed on such microemulsions. The elastic theory of the amphiphilic films always starts out from the assumption that the surfactant film will try to realize its spontaneous curvature c_0 in a given structure. Deviations from this spontaneous curvature will lead to an increase of the free energy of the system, which can be described in general by two elastic constants κ and $\bar{\kappa}$, the mean and the Gaussian bending elastic modulus (or saddle-splay modulus) [7]. The free energy F of such a system will then be given by (if we only take into account the bending energy F_b and an entropic contribution F_{ent}, and neglecting here the interfacial tension term)

$$F=F_b+F_{\text{ent}}=\int dA\,[(\kappa/2)(c_1+c_2-2c_0)^2+\bar{\kappa}c_1c_2] +NkTf(\Phi)\ , \tag{1}$$

where c_1 and c_2 are the two principal curvatures of the surfactant film. Accordingly the mean bending modulus κ should always be positive, since only in this case the spontaneous curvature is favored. The Gaussian modulus $\bar{\kappa}$ might either be negative, in which case droplet structures will be favored, or positive, which will favor saddle-splay structures as are found, for instance, in bicontinuous microemulsions, L_3 phases (sponge phases), or bicontinuous cubic phases. In the case of spherical droplets (of radius R) Eq. (1) reduces simply to (A is the total surface of all the droplets)

$$F/A=2\kappa(1/R-1/R_0)^2+\bar{\kappa}/R^2+[kT/(4\pi R^2)]f(\Phi)\ . \tag{2}$$

From the thermodynamic point of view the situation becomes particularly simple for the case in which the microemulsion phase is in equilibrium with the excess phase of the solubilizate. In that situation the droplets have achieved their maximum size, i.e., the maximum radius R_m, and no more of the solubilizate can be incorporated into the droplet phase. This situation where the solubilization capacity of the surfactant systems has been reached has been called the emulsification failure [10]. Any further addition of solubilizate will just add to the excess phase. Under this condition the minimization of the total free energy leads to a relation between the maximum droplet size R_m, the spontaneous radius $R_0=1/c_0$, and the elastic constants κ and $\bar{\kappa}$ [24]:

$$\frac{R_m}{R_0}=\frac{2\kappa+\bar{\kappa}}{2\kappa}+\frac{kT}{8\pi\kappa}f(\Phi)\ . \tag{3}$$

Here one may keep in mind that the dependence on the volume fraction Φ arises from also taking into consideration the entropy of the dispersion. Here as in all following expressions [Eqs. (3), (5), and (6)], for this entropy of mixing term $f(\Phi)$ we used the form proposed by Milner and Safran [25], i.e., a random mixing approximation [it might be noted here that we have chosen for convenience our $f(\Phi)$ to be $-h(\Phi)$ in their notation [25]]

$$f(\Phi)=(1/\Phi)\{\Phi\ln\Phi+(1-\Phi)\ln(1-\Phi)\}\ , \tag{4}$$

which reduces for small volume fractions to $\ln\Phi-1$, as has been used before to describe the entropic term [29] (see also Appendix B).

In addition, this theory may also yield an expression of the macroscopically observed interfacial tension at the planar interface between microemulsion and excess phases in terms of the elastic moduli and the maximum droplet size R_m [34]:

$$\gamma=\frac{2\kappa+\bar{\kappa}}{R_m^2}+\frac{kT}{4\pi R_m^2}f(\Phi)\ . \tag{5}$$

In a next step one may also consider thermal fluctuations of the microemulsion droplets. These fluctuations may be described by an expansion of the droplet deformation in terms of spherical harmonics Y_{lm} [23,25]. There it has been shown that the principal contribution to the fluctuations arises from the first two modes, i.e., $l=0$ and 2. For

the general case their mean square amplitudes are given by

$$\langle |u_0| \rangle^2 = \frac{kT}{6(2\kappa+\bar{\kappa}) - 8\kappa(R/R_0) + (3kT/2\pi) f(\Phi)} , \quad (6a)$$

$$\langle |u_2| \rangle^2 = \frac{kT}{16\kappa(R/R_0) - 12\bar{\kappa} - (3\kappa T/4\pi) f(\Phi)} . \quad (6b)$$

In this picture the zero order deformation described by u_0 is just the fluctuation in droplet size, i.e., changes of the mean droplet radius, or in other words the conventional polydispersity of the droplets.

The fluctuations described by u_2 are peanutlike deformations of the droplets that may be observed in dynamic measurements like the spin-echo experiment [35,36]. From Eqs. (6a) and (6b) it is clear that increasingly negative values for the saddle-splay modulus $\bar{\kappa}$ will have the effect of increasing the polydispersity of the droplets (by increasing u_0), while at the same time suppressing their shape fluctuations (that are characterized by u_2). For the case of the two-phase equilibrium we may insert Eq. (3) into Eq. (6a) in order to obtain the polydispersity index p simply as a function of the volume fraction and the elastic constants κ and $\bar{\kappa}$ (here we have implied that the observed polydispersity is just determined by the term u_0, as also stated in [26]. However, of course the higher order terms may also influence the deduced polydispersity, an effect that we will look at in more detail in Appendix A):

$$p^2 = \frac{u_0^2}{4\pi} = \frac{kT}{8\pi(2\kappa+\bar{\kappa}) + 2kTf(\Phi)} . \quad (6c)$$

This equation for the polydispersity implies a lower limit for the volume fraction (for given elastic constants) that the microemulsion can attain and remain stable (since p has to be finite, i.e., the denominator has to be positive): $\Phi > \exp[1 - 4\pi(2\kappa+\bar{\kappa})/kT]$. Equivalently one may arrive at a lower limit for $2\kappa+\bar{\kappa}$ for a given volume fraction, which will be given by $(2\kappa+\bar{\kappa}) > -f(\Phi)/4\pi$.

Therefore this description of the microemulsion properties by means of the elastic properties of the amphiphilic film yields the macroscopically observable interfacial tension as well as structural parameters like particle size and polydispersity. All these quantities are experimentally accessible (the structural parameters for instance by means of a small-angle-scattering experiment), and can therefore be used to verify this theoretical approach and obtain quantitative information regarding the corresponding elastic moduli.

B. Scattering theory for shell structured droplets

In most of the SANS experiments reported in the following we employed the shell contrast. This means that we used deuterated water and oil, and the surfactant remained the only hydrogenated compound. Since the scattering lengths of H and D are largely different, and determine the scattering length density of the given compounds, this means that the scattering length density [as defined by Eq. (7)] of the deuterated components will be very similar and at the same time differ largely from that of the surfactant. Therefore the scattering pattern of these samples will be mainly dominated by the amphiphilic film

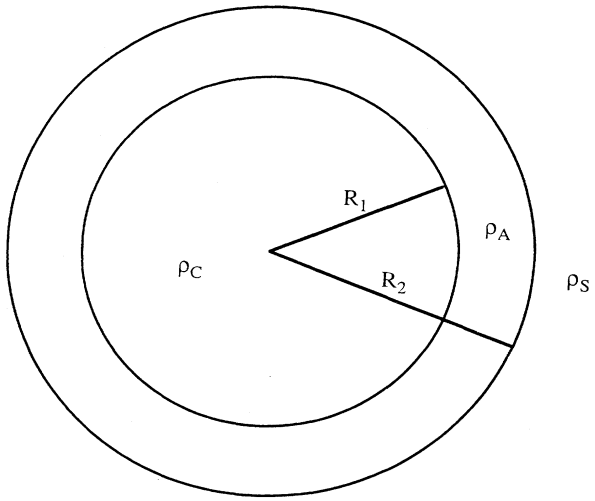

FIG. 1. Model of a shell structure microemulsion droplet (symbols described in the text).

$$\rho = \sum_i b_i / V , \quad (7)$$

where b_i is the scattering length of the given nuclei, and V is the volume of the given molecule, aggregate, etc.

For the case of droplet-type microemulsions this means that we may describe our droplets by means of a three-phase model, i.e., by assuming the presence of three different regions of scattering length density (Fig. 1): the core region that contains the solubilizate (oil for an O-W microemulsion), the shell that contains the surfactant, and the solvent phase. The scattering pattern for such a shell structured particle, i.e., its particle form factor, can easily be calculated for any number of concentric shells [37], and for our case may in general be written as

$$P(q) = 16\pi^2(\rho_A - \rho_S)^2 \{R_2^3 f_0(qR_2) - AR_1^3 f_0(qR_1)\}^2 \quad (8)$$

with

$$f_0(x) = (\sin x - x\cos x)/x^3 ,$$

$$q = (4\pi/\lambda)\sin(\Theta/2) ,$$

$$A = (\rho_A - \rho_C)/(\rho_A - \rho_S) .$$

R_1 is the inner radius of the droplet shell, R_2 is the outer radius of the droplet shell, and the scattering length densities are as follows: ρ_C: core; ρ_A: shell; and ρ_S: solvent.

This form factor applies to the monodisperse case but, of course, any real microemulsion system will exhibit some degree of polydispersity. In order to account for this polydispersity we allowed for a Schulz distribution $f(r)$ [Eq. (9)] [38] for the number size distribution of the aggregates. The Schulz function was centered around the

mean radius of the shell, while the shell thickness was kept constant. This assumption seems insofar reasonable since, according to the elastic theory, the size of the droplets should vary but the shell thickness should just be given by the length of the amphiphilic molecule and not vary much for the individual microemulsion droplets:

$$f(r)=\left[\frac{t+1}{R_m}\right]^{t+1}\frac{r^t}{\Gamma(t+1)}\exp\left[-\frac{t+1}{R_m}r\right], \quad (9)$$

with $t+1=1/p^2$. With this distribution function [Eq. (9)] we can now evaluate the scattering intensity of the polydisperse system according to

$$I(q)={}^1N\int_0^\infty f(r)P(q,r)dr\,S(q)\,, \quad (10)$$

where $r=(R_1+R_2)/2$, and ${}^1N$ is the number density of the aggregates. Within this model the scattering intensity is given by three adjustable parameters: the mean shell radius R_m, the shell thickness d ($=R_2-R_1$, which we assume to be fixed), and the polydispersity index p.

Up to now we have only considered intraparticle interferences, i.e., our $I(q)$ was simply obtained by summing over the intensity scattered by the individual particles. In reality, however, there will exist correlations between the individual droplets that lead to interparticle interferences, which will be considered by introducing the structure factor $S(q)$ [Eq. (11)]. This is why we have to multiply in Eq. (10) by $S(q)$. The simplest model for the structure factor $S(q)$ is the hard-sphere model that can be solved in the Percus-Yevick approximation to yield an analytical expression that depends only on the hard-sphere diameter σ and the volume fraction Φ (or equivalently on the number density) of the system [here $c(q\sigma)$ is the direct correlation function] [39]:

$$S(q)=\frac{1}{1-{}^1Nc(q\sigma)}\,, \quad (11)$$

$$c(q\sigma)=-4\pi\sigma^3\int_0^1 ds\,s^2\frac{\sin(sq\sigma)}{sq\sigma}(\alpha+\beta s+\gamma s^3)\,, \quad (12)$$

$$\alpha=\frac{(1+2\Phi)^2}{(1-\Phi)^4}\,,$$

$$\beta=-6\Phi\frac{(1+\Phi/2)^2}{(1-\Phi)^4}\,,$$

$$\gamma=0.5\Phi\frac{(1+2\Phi)^2}{(1-\Phi)^4}\,,$$

$$\Phi=(\pi/6)\,{}^1N\sigma^3\,.$$

Such a hard-sphere interaction should in general already be quite a good model for our microemulsion droplets since we employ only nonionic surfactants, which means that the main interaction between the aggregates should result from steric repulsion.

The introduction of this structure factor will add the diameter σ as a further parameter for the description of the scattering intensity. However, for our still not so highly concentrated systems $S(q)$ will in any way influence only the low-q part of the scattering curve, and not significantly alter its appearance in other parts. Therefore, in our investigations we never used the hard-sphere diameter σ as an individual parameter, but always fixed it to the particle radius as used for $P(q)$, which means that within this model there remain only three independently adjustable parameters.

All fits that are reported in the following were done for a model of a shell structure (sharp boundaries for the scattering length densities) with a constant thickness. We allowed for a polydispersity of the mean radius by assigning to it a Schulz distribution for the number size of the aggregates. This distribution function then should also contain the experimental smearing effects that result from the wavelength distribution of the neutrons, the finite size of the sample and detector elements, and the collimation effects of the primary beam. From the fits of the absolute scattering intensity the following three parameters were deduced: the mean shell radius R_m; the thickness of the shells, d; and the polydispersity parameter p ($p^2=\langle R^2\rangle/\langle R\rangle^2-1$). From the experimentally determined polydispersity parameter $p_{\rm exp}$ a corrected value p was obtained according to the equation $p^2=p_{\rm exp}^2-0.01$, thereby subtracting a value of 10% for the instrumental resolution function [29].

Such a procedure is insofar justified since both distribution functions should be roughly Gaussian-like. This holds for a not too broad Schulz distribution, and also the experimental resolution function in a SANS experiment has been shown to be well approximated by a Gaussian [40]. Yet for Gaussian functions the exponents of several Gaussian distribution functions applied to the same original function should according to the convolution theorem simply be additive with a Pythagoras equation as given above. Therefore the deduced polydispersity parameter p should directly be related to the polydispersity of the corresponding particles. It might be noted here that we also verified that our deduced parameters, i.e., R_m and p, do not depend in any significant way on the choice of the particular distribution function; i.e., a Gaussian distribution would yield identical values. In addition, we also verified that the use of a model of a diffuse shell model (of the scattering length density) for the amphiphilic film, as has recently been developed [41], and that should be a more realistic description of the situation also yields identical values.

IV. RESULTS AND DISCUSSION

In the following we will analyze the scattering patterns for various O-W microemulsions, compare them to the interfacial tension data, and interpret them in terms of the elastic theory for microemulsions. Our studies were principally performed on microemulsions that were in the two-phase equilibrium, and contained a small amount of excess oil phase. By doing so the saturation with the oil phase is guaranteed, and one works under conditions that can easily be reproduced. It should also be remarked that all the samples were quite remote in the phase diagram from critical points; i.e., one can expect to have well-behaved microemulsion droplets to be present in all the systems.

A. Variation of the surfactant chain length

In a first series of measurements we compare O-W microemulsions of the system C_nE_j–D_{22}-decane–D_2O, where we varied the surfactant chain length. For this purpose we employed C_8E_3, $C_{10}E_4$, and $C_{12}E_5$, in order to keep the balance between the hydrophilic *EO* head group and hydrophobic alkyl chain approximately constant, while the thickness of the amphiphilic film changes. The SANS spectra were taken under identical conditions at 10 °C and are given in Fig. 2. The concentration was always in the semidilute regime, i.e., a volume fraction between 0.076 and 0.084.

In Fig. 2 we divided the scattering intensity by the volume fraction in order to have a measure that is independent of the particle concentration. Since the particle radii are also very close (one may directly infer this from the fact that the minima of the scattering curves are located at very similar q values for all the samples—and the q value of these minima is related to the shell radius R_m by $q=\pi/R_m$, where $R_m=(R_1+R_2)/2$; compare Fig. 1) the overall intensity then should mainly be determined by the shell thickness. However, it is evident that the intensity and therefore also the thickness of the shell scales nicely with the chain length of the surfactant employed, just as one should expect it. In addition one may readily observe how the minimum that indicates the relatively low polydispersity of the droplets is becoming less pronounced with decreasing surfactant chain length. Already for C_8E_3 a minimum is no longer found, but only a flat part in the scattering curve.

The experimental data were fitted with the shell model described in Sec. III B, with the scattering length densities as given in Sec. II A. In all cases the scattering length density of the core (ρ_C) was assigned to be that of the hydrocarbon, that of the shell (ρ_A) to be that of the surfactant, and that of the solvent (ρ_S) to be that of D_2O. In addition we used a hard-sphere structure factor. Here the hard-sphere diameter was given by $2(R_m+d_h)+d$, where d_h should account for the hydration shell of the droplet and was taken to be 3 Å for C_8E_3, 4 Å for $C_{10}E_4$, and 5 Å for $C_{12}E_5$. Such a larger hard-sphere radius was introduced in order to take into account the oligoethyleneoxide chains that will protrude into the aqueous surroundings of the droplet. That the *EO* part of the amphiphile really extends largely into the aqueous region has, for instance, been shown by means of neutron reflectivity experiments on C_nE_j surfactants at the air-water interface [42]. By that process the aggregates will already "feel" the presence of the other aggregates at a distance somewhat larger than twice the radii of the "dry" aggregate. This means that the protusion of the ethyleneoxide head group leads to an increase of the effective hard-sphere repulsion, i.e., to an increase of the effective hard-sphere radius. The value for d_h was chosen in such a way as to reflect the relative length of the *EO* chain. However, we checked that the numerical choice of this parameter d_h did not change in any significant way the outcome of our fitting procedure, since for the volume fractions employed the hard sphere $S(q)$ is still not very pronounced. It might be noted here that even choosing d_h to be 0 (or even omitting the structure factor at all) would still basically lead to similar values for R_m, d, and p, but the quality of the fits, especially in the low-q range, would suffer.

The fitted curves are given as solid lines in Fig. 2, and the corresponding fit parameters are listed in Table I, together with the sample compositions. We observe that in all cases our simple shell model yields a very good description of the experimental data. It is interesting to note that all samples saturated with decane possess roughly identical mean shell radii between 50 and 55 Å. The obtained thickness d of the shells increases with the chain length of the surfactant, thereby giving the expected scaling for the thickness of the amphiphilic film. The polydispersity index p strongly decreases with increasing surfactant chain length, as has also been observed by means of time-resolved fluorescence probing of similar microemulsions [43].

In addition, we may use our knowledge of the sample

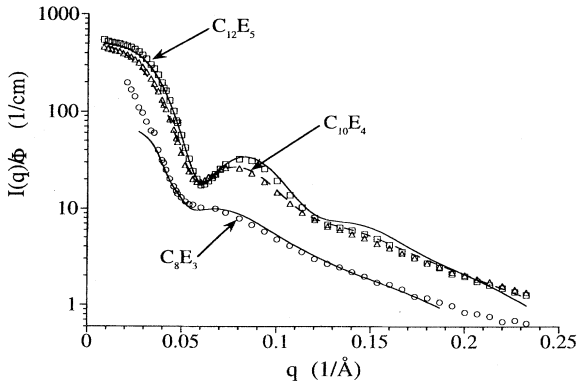

FIG. 2. SANS spectra (intensity in l/cm divided by the volume fraction) for O-W microemulsions of C_8E_3 (○), $C_{10}E_4$ (△), and $C_{12}E_5$ (□) with D_{22}-decane as oil in D_2O ($T=10$ °C). The solid lines are curves fitted with the shell model.

TABLE I. Mean shell radius R_m, shell thickness d, polydispersity index p, and head group area a_s for the oil saturated microemulsions in the system C_nE_j–D_{22}-decane–D_2O. Furthermore, the value for the interfacial tension γ at 10 °C is given (for these measurements we used D_2O but normal decane instead of the deuterated decane) together with the values for $2\kappa+\bar{\kappa}$ derived via p and γ, and the factor W [Eq. (14)].

Surfactant	C_8E_3	$C_{10}E_4$	$C_{12}E_5$
Φ	0.0841	0.078 42	0.076 49
R_m (Å)	55.6	50.4	49.1
d (Å)	11.0	13.0	15.2
p	0.2073	0.1409	0.1126
a_s (Å^2)	40.6	44.5	50.5
γ (mN/m)	0.0904	0.317	0.520
$(2\kappa+\bar{\kappa})(p)/kT$	1.20	2.28	3.42
$(2\kappa+\bar{\kappa})(\gamma)/kT$	0.90	2.34	3.50
W	0.772	1.028	1.022

composition together with the derived particle radii and polydispersity index in order to calculate the head group area a_s per surfactant molecule. For spherical droplets, simple geometry gives us

$$a_s = \frac{3}{R_m}\left[v_T + \frac{N_O}{N_T} v_O\right]\frac{1+p^2}{1+3p^2}\ , \tag{13}$$

where v_T is the volume of the hydrophobic part of the surfactant molecule (inside the aggregate) (we used 253 Å^3 for C_8E_3, 307 Å^3 for $C_{10}E_4$, and 362 Å^3 for $C_{12}E_5$). v_O is the volume of the oil molecule, N_T is the number of the surfactant molecules per volume, and N_O is the number of oil molecules per volume.

Here we consider only the hydrophobic part of the droplets. Therefore our head group area should apply to the surface of the aggregate where we have contact between the hydrophilic heads and the hydrophobic tails, i.e., a surface that should be located approximately at the midplane of the surfactant shell. The obtained values are listed in Table I, and we find that our values for a_s become smaller with decreasing size of the hydrophilic head group. They compare well to values that have been obtained by applying the Gibbs isotherm to surface tension data, which for $C_{12}E_5$ at 10 °C yielded (the same temperature at which we worked) a head group area of 48.6 Å^2 at the planar interface water/air [44]. In this investigation the same quantitative trend has also been observed; i.e., the value for a_s decreases with decreasing size of the hydrophilic moiety. At 10 °C for $C_{12}E_4$, 42.0 Å^2, and for $C_{12}E_3$, 39.3 Å^2 has been found. This means that the interpretation of our scattering data (and therefore also our droplet model) is in good agreement with the surface tension data. Furthermore, it seems evident that the area occupied by a surfactant molecule at the planar interface and that at the curved microemulsion interface (here we might recall that we used the midplane of the surfactant shell) are very similar. The head group area requirement of the surfactant molecule seems to be a universal quantity only slightly influenced by its actual state of aggregation.

With the help of these structural parameters in conjunction with the experimentally determined interfacial tension, one may now proceed to evaluate the elastic constants according to the relations outlined in Sec. III A. It is straightforward to calculate the parameter $2\kappa+\bar{\kappa}$ from the experimental polydispersity index p via Eq. (6c). We may equally well compute $2\kappa+\bar{\kappa}$ independently from the interfacial tension γ and the value for the droplet radius R_m via Eq. (5). The values calculated via both routes are given in Table I. Although here we start from experimental quantities that were determined completely independently, we arrive at values for the sum of the elastic constants $2\kappa+\bar{\kappa}$ that are in very good agreement.

The value for $(2\kappa+\bar{\kappa})/kT$ increases with increasing chain length of the surfactant from 1.0 for C_8E_3 over 2.3 for $C_{10}E_4$ to 3.5 for $C_{12}E_5$. Such an increase of the elastic constant with increasing chain length of the surfactant has been predicted by theory [45,46]. Accordingly the elastic constant should scale with the surfactant chain length l to the power 2.5–3. If we now calculate the length l by assuming an all-trans configuration of our surfactant molecules, we obtain values of 23.2 Å (C_8E_3), 29.3 Å ($C_{10}E_4$), and 35.5 Å ($C_{12}E_5$). According to this l^3 dependence one would therefore expect the value of the elastic constant to increase by a factor of 2.0 (3.6) while changing from C_8E_3 to $C_{10}E_4$ ($C_{12}E_5$). This scaling law is obviously well obeyed by our experimental data, which demonstrate how the value for $2\kappa+\bar{\kappa}$ really increases with increasing thickness of the surfactant film.

Finally one may use Eqs. (3), (5), and (6c) in order to eliminate the elastic moduli and the volume fraction dependence. By doing so one can write down an equation that directly interrelates interfacial tension γ, particle radius R_m, and polydispersity index p, and provides us with an experimentally accessible parameter W that according to theory should be identical to 1:

$$W = 8\pi p^2 \gamma R_m^2/kT = 1\ . \tag{14}$$

All these parameters have been determined experimentally for our systems, and if we calculate this factor W from Eq. (14) we find that for all our samples it lies in the range of 0.78–1.03 (Table I), i.e., a very good agreement between the predictions of the elastic theory for microemulsions and our data. This means that by knowing two of these three parameters (R_m, p, and γ) we can predict the third parameter with good precision. This already shows that the elastic theory for microemulsions described in Sec. III A is a powerful tool to explain the experimentally observable microemulsion properties.

Deviations from two-phase equilibrium

All theoretical expressions given in Sec. III A are derived for the case of a two-phase equilibrium between the microemulsion phase and the excess phase of the solubilizate. In the following we take a short look into what happens to the structural parameters if this condition is no longer fulfilled but if we consider microemulsions in the one-phase region, more or less far away from the phase boundary. There are principally two ways of moving away from the phase boundary. One is to increase the surfactant to oil ratio, the other to increase the temperature (which results in an increased solubility of oil in the microemulsion).

For this purpose we studied samples where we increased the ratio of surfactant to hydrocarbon, which means that correspondingly smaller aggregates are obtained since less oil will be solubilized per droplet. The recorded scattering curves are given in Figs. 3(a) ($C_{10}E_4$) and 3(b) ($C_{12}E_5$). In this context it is also interesting to note that the polydispersity seems to increase slightly as one moves away from the phase boundary, as indicated by the slightly less pronounced minima. The analysis with our shell model showed that the polydispersity index p increased from 0.141 to 0.146 for the $C_{10}E_4$ and 0.113 to 0.114 for the C_2E_5, i.e., it was only very little affected (compare Table II). Here it should be noted that this behavior is in evident contrast to the theoretical prediction given by Eq. (6a), according to which the polydisper-

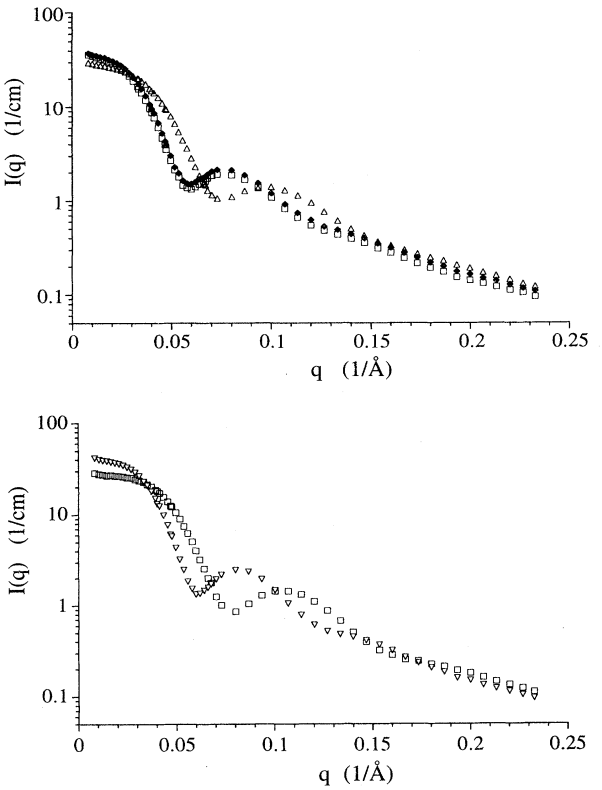

FIG. 3. (a) SANS curves for the system $C_{10}E_4$–D_{22}-decane at 10 °C. ◆: saturated sample. □: molar ratio of $C_{10}E_4$ to decane=0.694. △: molar ratio of $C_{10}E_4$ to decane=1.034 (all samples had a volume fraction of ~0.07). (b) SANS curves for the system $C_{12}E_5$–D_{22}-decane at 10 °C. ▽: saturated sample. □: molar ratio of $C_{12}E_5$ to decane=1.098 (all samples have a volume fraction of ~0.07).

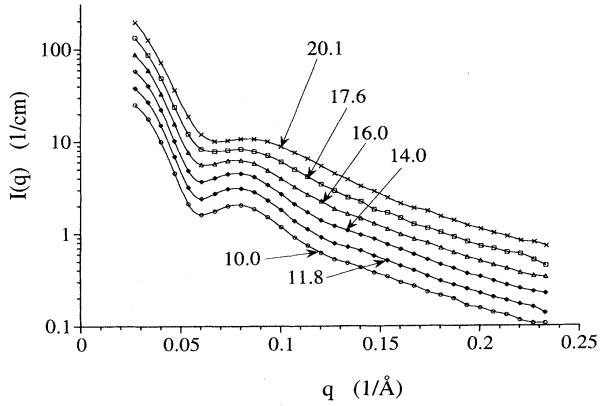

FIG. 4. SANS spectra for O-W microemulsions of the system $C_{10}E_4$–D_{22}-decane–D_2O as a function of the temperature (indicated in the plot in °C). The spectra are multiplied by a factor 2 in comparison to the correspondingly former spectrum at lower temperature for the purpose of better lucidity.

sity should decrease with decreasing particle radius. For instance in the case of $C_{10}E_4$ for the lowest oil/surfactant ratio the expected value for p would be 0.128, whereas from the SANS curves a value of 0.146 is deduced. This deviation is clearly beyond the experimental error and can so far not be accounted for by us.

In another investigation we studied the influence of increasing temperature on the scattering curves of the microemulsion system $C_{10}E_4$-decane (Φ: 0.0737). SANS spectra for various temperatures are given in Fig. 4, where it might be noted that at the lowest temperature (10 °C) the sample was still just in the two-phase equilibrium, whereas it was monophasic at all higher temperatures. From the spectra it is evident that the size of the droplets is only slightly affected, i.e., it is slightly reduced by the rise of temperature. At the same time the minimum in the curves becomes less pronounced, meaning that the polydispersity of the aggregates increases at the same time (compare Table III). Fits with the shell model yielded that the polydispersity index p rises from 0.141 (at 10 °C) to 0.185 (at 20.1 °C), i.e., a much more pronounced change than that observed in the case of changing the microemulsion composition, but in the same direction.

To summarize these results, it appears that the polydispersity of the droplets is not dramatically changed upon leaving the phase boundary, i.e., the two-phase equilibrium condition. Evidently the polydispersity is lowest for the two-phase equilibrium, and increases upon moving away from the phase boundary. Hardly any change is observed upon changing the sample composition, and the change is also still fairly small for temperature changes that are not too large. Although there exists a qualitative discrepancy for the change of the polydispersity upon decreasing the oil/surfactant ratio, its quantitative change is not very large. Therefore it would seem well justified to work in the one-phase region (not too far away from the phase boundary) and still apply theoretical expressions that would strictly only be valid for the situation of two-phase equilibrium.

B. Contrast variation experiment

In order to further verify our droplet picture for the O-W microemulsion we performed an external contrast

TABLE II. Mean shell radius R_m, shell thickness d, and polydispersity index p for the oil saturated microemulsions in the systems $C_{10}E_4$ or $C_{12}E_5$–D_{22}-decane–D_2O at 10 °C for various oil-surfactant ratios. Two-phase equilibrium was only present for the corresponding sample with the highest oil-surfactant ratio.

Surfactant	m(oil)/m(surfactant)	Φ	R in Å	d in Å	p
$C_{10}E_4$	0.713	0.0726	50.4	13.7	0.141
$C_{10}E_4$	0.708	0.0737	50.2	13.8	0.141
$C_{10}E_4$	0.475	0.0724	39.7	14.1	0.146
$C_{12}E_5$	0.606	0.0765	49.1	15.2	0.113
$C_{12}E_5$	0.368	0.0718	38.2	15.3	0.114

TABLE III. Mean shell radius R_m, shell thickness d, and polydispersity index p for the oil saturated microemulsions in the system $C_{10}E_4$–D_{22}-decane–D_2O at various temperatures. Two-phase equilibrium was only present for the sample at 10 °C.

T in °C	R_m in Å	d in Å	p
10.0	49.1	13.5	0.141
11.8	49.5	13.6	0.141
14.0	49.3	13.6	0.146
16.0	48.3	13.4	0.159
17.6	46.6	13.1	0.167
20.1	45.0	12.6	0.185

variation experiment on the $C_{12}E_5$–D_{22}decane–water system, i.e., we employed mixtures of D_2O and H_2O. The contrast variation method should also yield information regarding the polydispersity of the given droplets since the scattering intensity extrapolated to $q=0$, $I(0)$, at the matching point, i.e., the minimum scattering intensity, should be related to the polydispersity of the particles [47]. This determination of the polydispersity will be independent of the model employed for fitting the complete scattering curve, and therefore yield an independent value of p.

The investigated sample had a volume fraction (surfactant plus decane) of 0.0764, and eight different H_2O-D_2O mixtures were employed for the experiments. All scattering curves were corrected for the solvent background, using the corresponding arithmetic value for the given H_2O-D_2O mixture (according to their volume fraction in the system). The incoherent scattering resulting from the hydrogenated surfactant (and much less important of the deuterated oil) were corrected for by calculating the number density of the corresponding H and D atoms and using known values for the incoherent scattering length of the nuclei [$\sigma_{inc}(H)=79.9\times10^{-24}$ cm^2, and $\sigma_{inc}(D)=2.04\times10^{-24}$ cm^2 [48]]. In our case this correction for the incoherent scattering of the surfactant amounts to about 0.23 cm^{-1}.

The resulting scattering curves for the various solvent contrasts are plotted in Fig. 5. $I(0)$ was extrapolated from a Guinier approximation, i.e., $I(q)=I(0)-bq^2$, which holds in general for the low-q range, independent of the particle structure. In that connection it is also of no importance that the concentration of the particles cannot be considered to be ideally diluted, since the structure factor that has to be taken into account to describe the concentration effects will also show a q^2 dependence in the low-q range [49]. Therefore the influence of the structure factor will not change the linearity in q^2 but only change the proportionality factor b and still allow for a reliable extrapolation of $I(0)$.

At the same time all the intensities extrapolated to $q=0$ will be given by $P(0)$ times $S(0)$. For our microemulsion we may safely assume that the interaction between the droplets is mainly just steric (as they are uncharged), and can be described by a corresponding hard-sphere system. This assumption has also been verified above, where we showed that we can describe the scattering curve of these microemulsions perfectly well with the

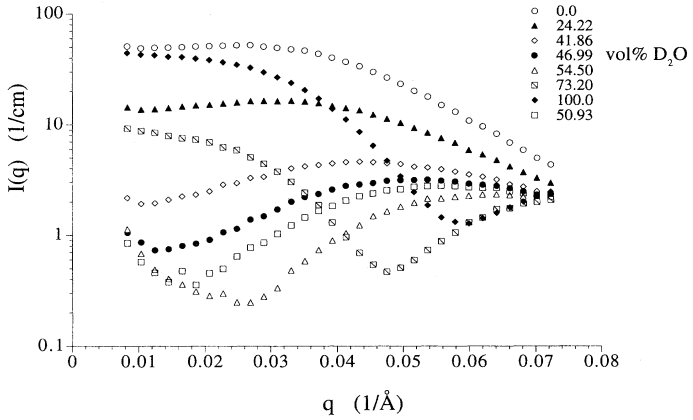

FIG. 5. SANS spectra for various contrast conditions in the system $C_{10}E_4$–D_{22}-decane-water at 10 °C. The volume fraction of D_2O in the D_2O-H_2O mixture is given.

hard-sphere structure factor. For such a system the Carnahan-Starling expression [Eq. (15)] has shown itself to be very well adapted [50]:

$$S(0)=\frac{(1-\Phi)^4}{(1+2\Phi)^2-4\Phi^3+\Phi^4}\ . \tag{15}$$

For our system with $\Phi=0.0764$ this leads to $S(0)=0.548$. It might be remarked here that the value of $S(0)$ bears no influence on the polydispersity index p that we will derive, since it is exclusively given by the ratio between the minimum intensity and $I(x=0)$. However, the choice of $S(0)$ will influence the absolute values for the radius and thickness (not their ratio) determined by the position of the intensity minimum. Division of the extrapolated intensity by the $S(0)$ value will then yield the proper zero scattering intensity that is directly given by the particle concentration ^1N times the particle form factor $P(q,r)$ (which at $q=0$ is just proportional to the square of scattering volume times the difference of the scattering length densities), which here has to be averaged for the case of polydispersity:

$$I(0)/S(0)={}^1N\langle P(0,r)\rangle\ . \tag{16}$$

The experimentally obtained values for $[I(0)]^{1/2}$ are plotted in Fig. 6 as a function of the contrast, and we find a minimum in that curve that differs distinctly from zero, which is the result of the polydispersity of the droplet that prevents the system from having one single matching point.

This scattering intensity at $q=0$ may now be evaluated for a system of polydisperse shells, i.e., we have to compute the average denoted by the brackets in Eq. (16). Here again we describe this polydispersity for the number density of the aggregates by a Schulz distribution of the radii [Eq. (9)] [38]. Then one may simply integrate the corresponding $q=0$ scattering intensity for the monodisperse case [which depends, of course, on the contrast conditions, and is given by Eq. (17)] over the distribution function and obtain an analytical expression for $I(0)$ [given by Eq. (18)]:

$$I(0)/S(0)={}^1N(16/9)\pi^2(\rho_A-\rho_S)^2[R_2^3-AR_1^3]^2\ , \tag{17}$$

$$\begin{aligned} I(0)/S(0)={}^1N(16/9)\pi^2(\rho_A-\rho_S)^2[&(1-A)^2B_5R^6+3(1-A^2)B_4R^5d \\ &+(15+6A+15A^2)i+B_3R^4d^2/4+5(1-A^2)B_2R^3d^3/2 \\ &+(15-6A+15A^2)B_1R^2d^4/16+3(1-A^2)Rd^5/16+(1+A^2)d^6/64]\ , \end{aligned} \tag{18}$$

with

$$B_n=\frac{\prod_{i=1}^{n}(t+i+1)}{(t+1)^n}\ .$$

Our $I(0)$ now depends on the mean radius R_m, the thickness d (which is constant in this model, i.e., again no dispersion of the shell thickness is assumed), the polydispersity parameter p (which is directly related to the corresponding parameter t of the Schulz distribution via $t+1=1/p^2$), and, of course, on the scattering length density of the solvent (here again we take for the scattering length density of the core and the shell those for D_{22}-decane and $C_{12}E_5$, respectively). In this expression R and d will be determined by the slope of $(I^{1/2})$ (or equivalently by the absolute values of the scattering intensity) as a function of the solvent composition x, the ratio of R to d will mainly determine the position to the minimum, and the depth of the minimum will be given principally by the polydispersity; i.e., all three parameters describe distinctively different features of the curve for $(I)^{1/2}=f(x)$, and can be determined independently with precision by this method.

In a next step we used Eq. (18) to fit the experimental data $I(0)/S(0)$, and a very good agreement between the fit (solid line) and the data (Fig. 6) is observed. From this fit procedure a radius $R_m=48.7\pm1.1$ Å, a thickness $d=14.8\pm0.4$ Å, and a polydispersity index $p=0.134\pm0.017$ can be deduced. These values compare very well with those obtained from the fit of the corresponding angle-dependent scattering curve of the same system in pure D_2O (cf. Table I). The coincidence of the values of the polydispersity derived from two completely different approaches also verifies the validity of our procedure to deduce p from the q-dependent scattering curves (especially the proper taking into account of the experimental resolution). A similar approach has been used before [29], but in the present study the range around the matching point has been investigated in more detail and we also use the precise formula Eq. (18) for our shell model to fit our data.

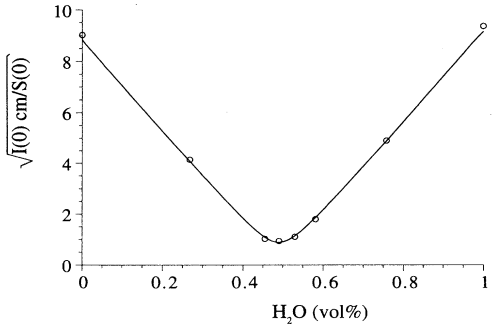

FIG. 6. Square root of $[I(0)/S(0)\ (l/\text{cm})]$ as a function of the solvent mixture for the contrast variation in the system $C_{12}E_5$–D_{22}-decane–(D_2O-H_2O).

Here it is interesting to note that the value for the polydispersity obtained this way is principally different from that deduced from a fit of the angle-dependent scattering curve since there the instrumental resolution function is of principal importance. The instrumental resolution function results in a smearing of the first minimum (and of course also of higher minima, that are, however, much less pronounced in any case) that is similar to the effect of polydispersity. Therefore one has to account properly for the instrumental smearing in order to derive realistic values for the polydispersity index.

This problem does not arise at all for the analysis of the contrast variation data, since $I(0)$ is independent of the experimental resolution. The main experimental uncertainty that remains is the proper knowledge of the incoherent background, since around the matching point the incoherent scattering will be of about the same order of magnitude as the coherently scattered part. However, one can experimentally easily determine the incoherent scattering of the solvent, whereas for the incoherent scattering that results from colloidal particles (especially from their hydrogenated components) some uncertainty remains, which will then limit the precision of the obtained polydispersity parameter. However, the contrast variation method should normally be quite accurate (even for the lowest scattering intensities we judge our error to be less than 10%), and only become somewhat more imprecise for p values significantly smaller than 0.1 (since here very low coherent scattering intensities are to be expected around the matching point, which will be more difficult to discern from the incoherent scattering).

Finally we might note that two different evaluations of the polydispersity (via the shape analysis and the contrast variation method) are also fundamentally different in that in the contrast variation the polydispersity of the volume of the aggregates is exclusively probed, independent of the actual shape of the aggregates. Here we may again employ the model where the deformation of the spherical droplets is described by an expansion in spherical harmonics $Y_{lm}(\theta,\phi)$ [23]:

$$R(\theta,\phi)=R_m\left[1+\sum_{l,m}u_{l,m}\,Y_{l,m}(\theta,\phi)\right]\ . \tag{19}$$

With this, and using the definition of the polydispersity index p, we may readily write p in terms of the expansion

coefficients u_l (where we omit the u_l term since it represents only a translation of the droplets [23], and then neglect terms higher than second order) as

$$p^2=\frac{\langle (R-R_m)^2\rangle}{R_m^2}=\frac{1}{4\pi}\sum_{l\neq 1}(2l+1)\langle |u_l|^2\rangle \approx\frac{\langle |u_0|^2\rangle+5\langle |u_2|^2\rangle}{4\pi}. \quad (20)$$

Accordingly the polydispersity should be larger than that given by u_0, as we have assumed so far. In Appendix A we show that the polydispersity actually derived from the shape analysis of the SANS curves should indeed yield a somewhat lower value than given by Eq. (20) (although it will be somewhat increased by the shape fluctuations). This is in agreement with our experimental data, where from the shape analysis we find $p=0.113$, whereas the contrast variation, that should reflect the volume polydispersity, yields the larger value $p=0.134$. Of course, the evaluation of the polydispersity in both cases is associated with a certain incertitude, but the experimental data seem to reflect the proper direction of this effect.

C. Variation of the hydrocarbon chain length

In this part we want to investigate the influence on the employed hydrocarbon on the microemulsion structure, i.e., its influence of the bending properties of the amphiphilic film. For this investigation $C_{10}E_4$ was used as a surfactant. The surfactant concentration was always around 3.3 wt %, thereby yielding a volume fraction (of oil plus surfactant) between 0.08 (for decane) and 0.105 (for hexane) for the oil-saturated samples. The SANS data for the various samples are given in Fig. 7 together with the fitted curves as solid lines. For the fits, the shell model as described in Sec. III B was again employed in conjunction with a hard-sphere structure factor, and this model describes the data very well in all parts of the scattering curves (solid lines in Fig. 7). The scattering length densities used are all given in Sec. III A. The deduced structural parameters for the aggregates are summarized in Table IV. Furthermore, we also calculated the head group area a_s per surfactant molecule at the midplane of the surfactant shell according to Eq. (14). The values are also given in Table IV, and we find that a_s remains relatively constant and does not change in a systematic manner with changing hydrocarbon chain length.

In this series one observes that with decreasing chain length of the hydrocarbon, larger amounts of it can be solubilized, which manifests itself in an increasing particle radius. This effect is quite pronounced, and the mean shell radius R_m increases from 50 Å for decane to about 90 Å for hexane, which means that about twice the amount (by volume) of hexane in comparison to decane can become solubilized by the same amount of surfactant. A similar tendency has been reported before for other nonionic surfactants [51]. The obtained shell thickness stays constant in the range 12–13 Å, a reasonable value for $C_{10}E_4$. Furthermore, it is interesting to note that the polydispersity of the microemulsion droplets remains unchanged at 14.0% independent of the oil used. Therefore the polydispersity, which should directly be determined by the bending elasticity, is independent of the type of hydrocarbon employed in the microemulsion. We mention here that such an independence of the elastic constants from the oil chain length does not necessarily hold in general, since it has been found, for instance, by ellipsometric measurements in the system aerosol OT AOT-brine that κ may change dramatically with the increasing chain length of the hydrocarbon [52].

However, the constant value that we find seems to be reasonable, as the bending elasticity of the interface should mainly be determined by the surfactant film that forms this interface, and only minor influences of the solubilized oil on the elastic properties of this interface might be expected. Fluorescence probing experiments in the system $C_{12}E_5$-decane and heptane also showed a similar polydispersity for both oils [43]. Of course, the solu-

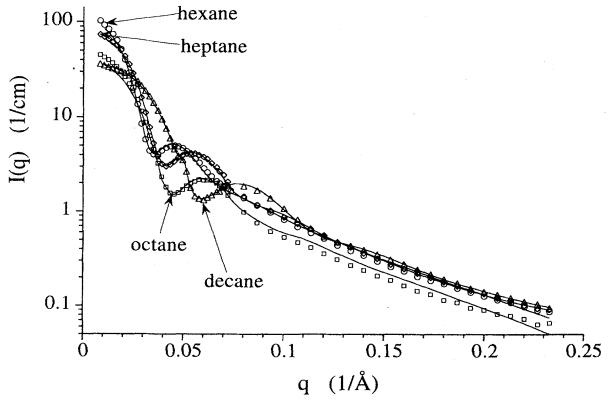

FIG. 7. SANS curves of microemulsions composed from $C_{10}E_4$ in D_2O and various oils: D_{14}-hexane, D_{16}-heptane, D_{18}-octane, and D_{22}-decane (taken at 10 °C). The solid lines are the fitted curves.

TABLE IV. Mean shell radius R_m, shell thickness d, polydispersity index p, and head group area a_s for the saturated microemulsions composed of $C_{10}E_4$ and various deuterated oils (taken at 10 °C). In addition, the value for the interfacial tension γ at 10 °C is given (for these measurements we used D_2O but normal oils instead of the deuterated oils) together with the values for $2\kappa+\bar{\kappa}$ derived via p and γ, and the factor W [Eq. (14)].

Oil	Decane	Octane	Heptane	Hexane
Φ	0.078 42	0.080 16	0.094 77	0.104 46
R_m in Å	50.4	67.2	74.8	88.7
d in Å	13.0	11.2	13.1	12.6
p	0.1409	0.1396	0.1398	0.1404
a_s in Å^2	44.5	45.1	46.0	43.9
γ in mN/m	0.317	0.214	0.139	0.0852
W	1.028	1.211	0.980	0.850
$(2\kappa+\bar{\kappa})(p)/kT$	2.28	2.32	2.30	2.27
$(2\kappa+\bar{\kappa})(\gamma)/kT$	2.34	2.75	2.26	1.97

bilization of a substrate into a microemulsion system will normally also be related to the macroscopically observable interfacial tension between this substrate and the microemulsion. The experimentally obtained interfacial tensions are also given in Table IV, and correlate well with the observed droplet radii. The lower the interfacial tension γ the higher the solubilization capacity for this oil, hence the larger the droplet radii of the saturated aggregates.

Furthermore, we may use Eq. (14) and again calculate the factor W defined there. By doing so we find W to be in the range of 0.8–1.2 for all our samples (Table IV), i.e., again a very good agreement between the predictions of the elastic theory for microemulsions and our data, as already similarly observed in Sec. II A. Evidently this relation applies quite universally for droplet microemulsion systems.

Again as described in Sec. IV A, we may obtain two independent values for the factor $(2\kappa+\bar{\kappa})$ by using, in one case, the experimentally obtained polydispersity index p via Eq. (6c) and, in the other case, the macroscopic interfacial tension γ (in conjunction with the R_m value obtained from SANS) together with Eq. (5). The corresponding values are also given in Table IV, and as already expected above we find that the value deduced via p remains constant around 2.3 kT for all oils employed. The values derived via the interfacial tension are more scattered (most likely due to the individual errors for the measurement of the interfacial tension, whereas in comparison p is deduced from the scattering curves, where the relative error is small), and range between 1.97 and 2.75 kT, yet are on average still in very good agreement with the values obtained from p. This means that the sum of the elastic bending constants $(2\kappa+\bar{\kappa})$ is not significantly affected by the change of the solubilized oil, i.e., the elastic properties of the amphiphilic layer seem to be dominated by the properties of the amphiphile and only slightly influenced by the choice of the oil. As mentioned above this does not necessarily hold in general (compare [52]) and one may expect significant changes for the case in which the chain length of the oil becomes larger than that of the surfactant. It should also be mentioned that it has been shown for W-O systems that here the chain length of the oil may strongly affect the droplet interactions [53].

D. Dilution series for O-W droplets of the system $C_{10}E_4$-decane at 10.0 °C

In a next step we investigated the concentration dependence of the structural parameters, since according to Eqs. (3) and (6c) they should depend on the microemulsion volume fraction. For this study we chose the $C_{10}E_4$-decane system. The samples were prepared simply by diluting the most concentrated sample with D_2O since the critical micellar concentration (cmc) for this surfactant is sufficiently low to be neglected (0.68 mM at 25 °C [54]). Again all samples were in equilibrium with a small amount of excess oil phase.

A plot of all the experimental data for this dilution series is given in Fig. 8. One finds that the minimum that

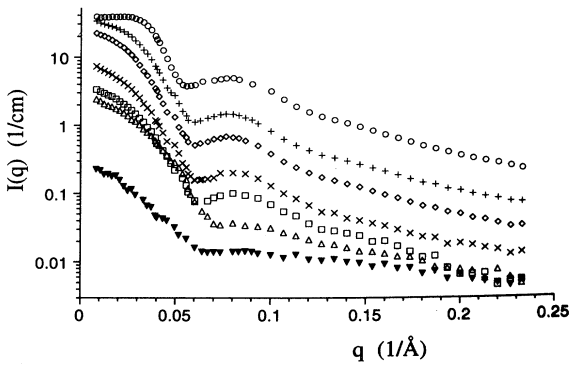

FIG. 8. SANS curves for a dilution series of the O-W microemulsion system $C_{10}E_4$–D_{22}, decane–D_2O at 10 °C. (volume fractions: ○ 0.2098; +: 0.0670; ◇: 0.0309; ×: 0.009 97; □: 0.004 86; △: 0.00209; ▼: 0.000 681).

indicates the particle size is somewhat shifted to higher q with decreasing concentration, which shows that the aggregates become smaller. At the same time this minimum becomes less pronounced, a sign that the polydispersity of the aggregates is increasing.

The scattering curves could again all very well be described by the shell model, using a hard-sphere model for the structure factor (which is, of course, only important for the sampless which a volume fraction of more than 5%). This analysis of the scattering curves yields a continuous decrease of the droplet size with decreasing concentration, as to be expected from Eq. (3) of the microemulsion theory [24]. At the same time the deduced polydispersity index is monotonously increasing from 0.133 to 0.209, an effect that is also in good agreement with the predictions of the theory [Eq. (6c)]. The obtained data are summarized in Table V. It should be mentioned here that in a recent study [55] on the W-O microemulsion in the system sodium dodecyl sulfate (SDS)–cyclohexane–brine–pentanol or hexanol just the opposite tendency has been claimed, i.e., an increase of polydispersity with increasing concentration. Evidently this point has still to be clarified, since one should expect this to be a general property of microemulsion droplet systems. Yet for our system, given the SANS data, the

TABLE V. Dilution series for $C_{10}E_4$–D_{22}-decane-D_2O (at 10 °C) (mass ratio $C_{10}E_4$–D_{22}-decane=0.834, but a small amount of excess oil is present). Given are the mean shell radius R_m, the shell thickness d, and the polydispersity index p (corrected for the experimental resolution).

Φ	R in Å	d in Å	p
0.2098	54.4	13.0	0.1329
0.0670	50.5	12.2	0.1436
0.0309	50.4	12.4	0.1473
0.009 97	48.2	12.0	0.1560
0.004 86	46.8	12.3	0.1596
0.002 09	41.1	13.7	0.1890
0.000 681	41.5	13.1	0.2093

trend is unequivocaly a decrease of polydispersity with increasing concentration, a trend that is furthermore predicted by theory.

According to Eq. (3) the radius R should scale linearly with $f(\Phi)$, i.e., correspondingly decrease with increasing dilution. The deduced radii R are given in Fig. 9(a) as a function of $f(\Phi)$ [as defined by Eq. (4)], and a reasonable linearity is observed. Here we used the mean shell radius since this should give approximately the plane that separates hydrophobic and hydrophilic parts (if we keep in mind that the size of the alkyl chain and the hydrophilic part of the surfactant are nearly equal). The fit of a straight line to the data gives values of 60.0 for $R_0(2\kappa+\bar{\kappa})/2\kappa$, and 2.37 for $R_0kT/(8\pi\kappa)$ [$\Longrightarrow R_0/\kappa$ (in Å/kT)$=59.6$]. These values seem to be reasonable since R_0 can probably be expected to be in the range of 60–80 Å which would yield a κ value of roughly 1 kT. Furthermore, we can directly obtain from these values that $2\kappa+\bar{\kappa}$ is 2.02 kT, a value that is in good agreement with the values that we had before deduced from the polydispersity and the interfacial tension data (in connection with the particle radius) in Sec. IV A (cf. Table I). It should be noted here that this evaluation from the dilution series is completely independent from the analysis discussed in Sec. IV A, and therefore presents a strong corroboration of the fact that our value for $2\kappa+\bar{\kappa}$ is really reliable.

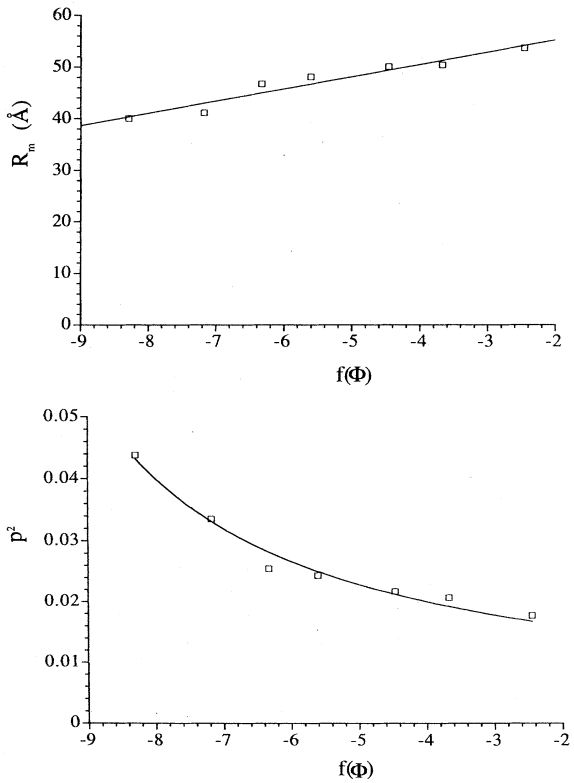

FIG. 9. (a) The particle radii (mean shell radii) as a function of $f(\Phi)$ for the system $C_{10}E_4$-D_{22}-decane–D_2O at 10 °C (Φ: volume fraction of surfactant plus oil). (b) p^2 as a function of $f(\Phi)$ for the system $C_{10}E_4$–D_{22}-decane–D_2O at 10 °C (Φ: volume fraction of surfactant plus oil; p: polydispersity index).

According to Eq. (6c) the polydispersity index p should have an inverse relation to $f(\Phi)$, i.e., p should increase with decreasing concentration. The corresponding plot for the experimental data [p^2 as a function of $f(\Phi)$] is given in Fig. 9(b). These experimental data we have fitted with a formula of the type $1/[a+bf(\Phi)]$, which corresponds to Eq. (6c) [the solid line in Fig. 9(b) corresponds to fitting all the points]. We find that this formula is roughly able to describe the experimental data, keeping in mind that, of course, the determination of the polydispersity index p contains a larger uncertainty than for the radii. The value obtained this way for $2\kappa+\bar{\kappa}$ (2.75 kT for fitting all points, 2.44 kT if we skip the two points at lowest concentration since they are somewhat less reliable) is in reasonable agreement with the values obtained above by analyzing the radius dependence and also with the results from Sec. IV A. However, the factor for b is almost always significantly larger than the 2 predicted by Eq. (6c), i.e., 6.56 for all points and 4.37 if we skip the first two points.

This means that the experimental values for p change much more than predicted by theory. This should not be due to our procedure of obtaining the particle polydispersity index p by subtracting the experimental resolution (see Sec. III B) since judging from the comparison with the polydispersity index obtained via the contrast variation method this procedure seems to be well justified. There evidently remains a marked discrepancy between the theory and the change of the polydispersity values, whereas for the same samples the expected relation for the radii seems to be well fulfilled. This so far unresolved discrepancy will be addressed in future investigations.

V. CONCLUSIONS

For our microemulsion system composed of the nonionic surfactant alkyloligoglycolether C_nE_j, hydrocarbon, and water, it has been shown that in the O-W microemulsion the bulk structures and interfacial tension values can be described very well in terms of the bending properties of the amphiphilic film. SANS experiments in the shell contrast (deuterated oil and water) could be fitted very accurately with a model of polydisperse spherical shells, and allowed for a precise determination both of the shell radius and the polydispersity index p. The reliability of the procedure to obtain p was verified independently by a contrast variation experiment where we deduced p from the scattering intensity at the matching point, a method that is independent of the experimental resolution (i.e., especially the wavelength spread of the employed neutrons).

All our experiments were performed on samples that were just in two-phase equilibrium, i.e., contained a small amount of excess phase. However, we also verified that the structural properties (especially the polydispersity index) of the droplets do not significantly change upon going into the one-phase region, as long as one is not very far away from the phase boundary. Here we encountered the problem that with decreasing particle radius (achieved by decreasing the oil/surfactant ratio) our deduced polydispersity index slighly increases, whereas ac-

cording to theory it should become smaller. So far we have no explanation for this effect, but will address this problem in future studies. In general we found the polydispersity to be lowest for samples in the two-phase equilibrium, and that it increases upon away from the phase boundary.

The observed droplet radii, polydispersity index p of the droplets, and the macroscopic interfacial tension at the planar interface can be related to the bending modulus κ and the saddle-splay modulus $\bar{\kappa}$ of the amphiphilic film. The evaluation of the sum of the bending moduli $2\kappa+\bar{\kappa}$ by using, in one method, the polydispersity and, in another independent way, the aggregate radii in conjunction with the interfacial tension, leads to values that are in good agreement. This means that both methods seem to allow for a reliable calculation of the elastic film properties. In addition, this enables us to predict one the three quantities (R, p, or γ) if the other two are known to us.

Upon changing the chain length of the surfactant for a given hydrocarbon the droplet size remains roughly constant, while the polydispersity decreases significantly upon increasing the surfactant chain length. We observe that $2\kappa+\bar{\kappa}$ scales approximately with the chain length to the power 3, a result that has been predicted from theory for the elasticity of an amphiphilic film, and that has now been verified by us experimentally. A change of the chain length of the hydrocarbon (in our case we varied from hexane to decane) shows that the droplet size increases for shorter hydrocarbons, whereas the polydispersity remains constant. Evaluation of the elastic constants showed that they are hardly influenced by the choice of the hydrocarbon. At least for this system the elastic properties seem to be exclusively determined by the surfactant employed.

Finally we performed a SANS experiment on a dilution series of these O-W droplets to verify the concentration dependence of the structural properties (R and p). Upon dilution the particle radii decrease and the polydispersity increases, as predicted by the elastic theory. From these changes again the sum $2\kappa+\bar{\kappa}$ can be evaluated, and is in good agreement with the values obtained above. The concentration dependence arises from the entropic contribution to the free energy of the system and comparison of various different expressions for the entropy of mixing leads us to the conclusion that a term corresponding to a random mixing approximation seems to be the most appropriate one for the description of our microemulsion droplets (see Appendix B). It should be noted here that the question of the appropriate term for the entropy of mixing for microemulsion droplets is still open. In particular recent work by Milner and Morse [56] indicate that there should be correction terms of the type $\ln(R/a)$, where a is a microcopic length which might significantly change the absolute value for the entropy of mixing (i.e., making it smaller). However, one problem in this context remains unresolved, which is the fact that the polydispersity changes as a function of the concentration much more than expected according to theory. So far we have no explanation for this effect but we will look in some more detail into this problem in future experimental investigations.

In summary we may state that the elastic theory of the amphiphilic film is a powerful tool for understanding microemulsion microstructure as well as macroscopic properties like the interfacial tension. For the systems studied by us these properties are quantitatively interrelated by the elastic theory, and this theory allows for a precise prediction of these properties in terms of the elastic constants of the surfactant film.

ACKNOWLEDGMENTS

This project was supported by a grant of the CEC (ERB4050PL920671). In addition, M. G. was supported by the Human Capital and Mobility program (ERB4001GT931413), financed by the European Community, that allowed him to participate in this project. We are grateful to J. Texeira, A. Brulet, and L. Noirez for help with the SANS experiments, and we would also thank S. Safran and R. Strey for helpful discussions. Finally we want to acknowledge P. D. Fletcher for communicating results to us prior to publication.

APPENDIX A: INFLUENCE OF FLUCTUATIONS ON THE SCATTERING CURVE— INTERPRETATION IN TERMS OF POLYDISPERSITY

In this part we will look at the influence of shape fluctuations of the microemulsion droplets on their scattering behavior. Such thermal fluctuations will cause the originally spherical aggregates to deviate from the spherical form. However, the particle form factor for such fluctuating droplets has been calculated before [36]. Of special importance is how it modifies the scattering pattern around the minimum of the form factor, since from that region we determined the polydispersity index p that we used extensively for the interpretation of our data. Of course, one would expect that form fluctuations will have a similar effect on the form factor as an increase of the apparent polydispersity since, for instance, ellipsoids (which one may think of as deformed spheres) show very similar scattering patterns as polydisperse spheres [57].

In order to estimate this effect we used the form factor for infinitely thin shells as given by [note that there is some correction to [36] in the term of $f_0(x)$]

$$P(q)=\left\langle V_s(\Delta\rho)^2\left[f_0(qR)+\sum_{l\geq 2}\frac{2l+1}{4\pi}f_l(qR)\langle|u_l|^2\rangle\right]\right\rangle_R , \tag{A1}$$

with

$$f_0(x)=j_0^2(x)+j_0(x)\sum_{l\geq 2}\frac{2l+1}{4\pi}\langle|u_l|^2\rangle \times\{(2-x^2)j_0(x)-2xj_l(x)\} ,$$

$$f_l(x)=[(l+2)j_l(x)-xj_{l+1}(x)]^2 ,$$

where $j_l(x)$ are the spherical Bessel function of lth order, and the large bracket stands for the averaging over the distribution function of the radii (conventional po-

lydispersity of the radii as described by u_0).

Here for simplicity we use the model for an infinitely thin shell; however, this does not impair the general validity of our conclusions since the form factor is only slightly modified if one goes to finite thicknesses, as long as the thickness remains significantly smaller than the particle radius, a restriction that has always been well fulfilled by the systems we investigated experimentally.

In the following we simulated scattering curves for fluctuating droplets by keeping only the $l=2$ term in the sum of Eq. (A1) since the higher order terms should be of minor importance [25], and we also checked this numerically. For the distribution function of the radii we used a Schulz distribution as in the main part of the paper. Such simulations were done for a variety of values of the polydispersity index p (0.05–0.3) and u_2 (0.025–0.5), and some examples are shown in Fig. 10. It is clearly observed that the increase of u_2 diminishes the extent of the minimum of the form factor, thereby mimicking an increased polydispersity.

In order to quantify this effect we subsequently fitted the calculated scattering curves with the form factor of rigid thin shells under exactly the same conditions as were used for fitting the experimental data. The fitting was performed in the range $0.9<qR<6$, i.e., in the range typically observed in a small-angle-scattering experiment, and where one has well centered the minimum of the form factor. Unless u_2 becomes too large (this means 0.2 for $p=0.05$ and changes to 0.4 for $p>0.2$) the simulated curves can always be fitted very accurately (by an apparent polydispersity index $p_{\rm app}$), and for too large u_2's the approximations made for deriving Eq. (A1) should no longer hold. That this is really the case can also be seen from the fact that for such high-u_2 values negative values for $I(q)$ may appear in the higher-q range, something which is, of course, an unphysical result.

In Fig. 11(a) we plot the obtained ratio of the apparent polydispersity index $p_{\rm app}/p_0$ versus the p_0 used originally for the simulation of the data for various assumed values of u_2. From looking at this plot it is evident that for low polydispersities the influence of u_2 can become quite significant, and increases the apparent polydispersity markedly. For the larger polydispersities this no longer holds, and $p_{\rm app}$ is hardly influenced in these cases. However, we can further reduce the uncertainty about this effect since u_2 and u_0 are both derived from the elastic moduli (and the concentration dependence via the entropic term) and are not independent of each other [cf. Eqs. (6a) and (6b)]. Inserting in Eqs. (6a) and (6b) the relation for R/R_0 [Eq. (3)], that holds for two-phase equilibrium, one obtains

$$\frac{u_2^2}{u_0^2}=\frac{2(2\kappa+\bar{\kappa})+(kT/2\pi)f(\Phi)}{4(4\kappa-\bar{\kappa})-(kT/\pi)f(\Phi)} . \tag{A2}$$

From this one may now estimate their relative magnitude. For droplet systems one may expect $\bar{\kappa}$ to be negative since that stabilizes such a droplet topology, and at the same time the entropic term $f(\Phi)$ necessarily has to be negative (since the free energy connected with the mixing process has to be negative). With these provisions it is obvious that u_2 always has to be smaller than $u_0/2$. Since $u_0^2=4\pi p_0^2$ we can conclude that u_2 should never

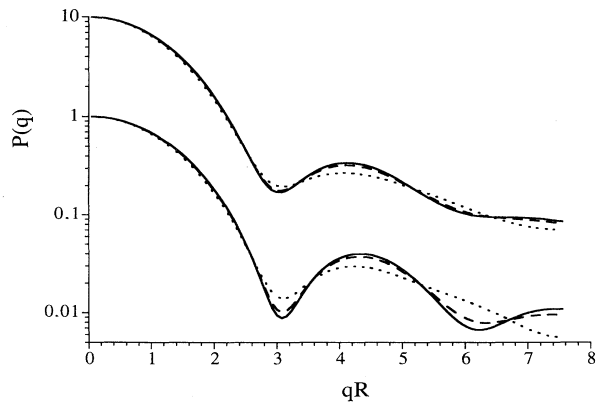

FIG. 10. Simulated particle form factors $P(q)$ for infinitely thin, fluctuating shells for $p=0.1$ (lower curves) and $p=0.15$ (upper curves). u_2 was chosen to be 0 (solid lines), 0.1 (long dashes), and 0.2 (short dashes).

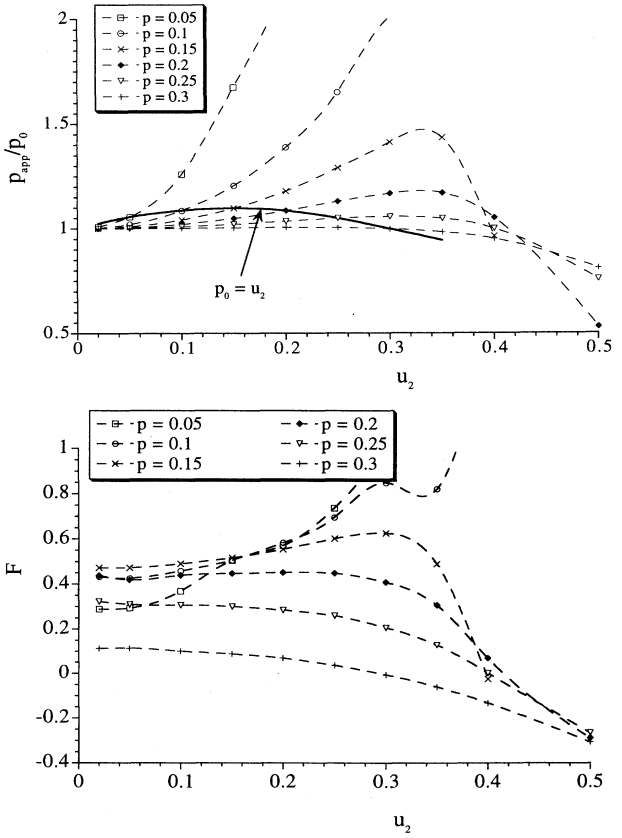

FIG. 11. (a) The ratio of the apparent polydispersity index (obtained from fitting the simulated curves) and input polydispersity index $p_{\rm app}/p_0$ as a function of u_2 for various inputs p_0. (b) The factor $F=(p_{\rm app}^2-p_0^2)/(5u_2^2/4\pi)$ as a function of u_2 for various inputs p_0.

exceed $1.75p_0$. This supplies us with an upper limit for the possible u_2 and, depending on the actual values for κ, $\bar{\kappa}$, and $f(\Phi)$, it may still be significantly smaller. Actually spin-echo experiments on a different sort of microemulsion droplets (W-O of AOT-butanol-decane-water) showed that there $\bar{\kappa}$ is close to -1.9κ [36]. A similar value of -1.75κ was also deduced for the O-W microemulsion of the AOT-heptane-brine system by analysis of interfacial tension data [34]. However, for such values the relative importance of u_2 in comparison to u_0 becomes very small, and is negligible in changing the apparent polydispersity.

We indicate this limit of the effect of u_2 on the apparent polydispersity in Fig. 11(a) by means of a solid line that is drawn for the case of $u_2=p_0$, which should not be to far from a realistic upper limit for u_2. For that case the change of the apparent polydispersity would still always be less than 10%. However, in our systems we estimate $\bar{\kappa}$ contributes significantly, thereby rendering the relative importance of u_2 even less significant. This estimation is vindicated by the fact that the values derived for $2\kappa+\bar{\kappa}$ by way of the polydispersity index are always close to those deduced from interfacial tension γ and radius R (compare Tables I and IV), where the latter value would not be influenced by the value of u_2. Therefore it seems to be justified to equate p with the corresponding expression that relates u_0 to the elastic constants as we have done in Eq. (6c), and as used throughout the paper. Of course, such an assumption does not necessarily have to be valid in general, and one might imagine systems where conditions could be different.

Finally we may judge the influence of u_2 on the apparent polydispersity by a comparison with the prediction according to Eq. (20), derived from the same model for fluctuating particles where this fluctuation is described in terms of spherical harmonics. For that purpose we have plotted in Fig. 11(b) the factor $F=(p_{\rm app}^2-p_0^2)/(5u_2^2/4\pi)$, which should be a measure of how large the influence of u_2 is on the deduced $p_{\rm app}$. If Eq. (20) would hold, this factor should be unity, but from looking at Fig. 11(b) one finds that it always remains much smaller than 1. For realistic situations in microemulsion systems (cf. above) this factor seems to be between 0.1 and 0.5, which means that Eq. (20) clearly overestimates the polydispersity that one will derive from a shape analysis of the SANS curves. This again proves that our method of relating the derived polydispersity index to the u_0 term of the expansion seems to be well justified, since the other terms contribute only marginally to the deduced polydispersity.

APPENDIX B: ENTROPY TERM IN MORE DETAIL

Here we want to address the influence of the entropy term in the free energy expression [Eq. (1)] on the interpretation of our experimental data. In the main paper we always used a specific form for the entropic term [given by Eqs. (4) or (B1)]. However, this term is by no means unequivocally agreed upon, and several other expressions for the mixing entropy of microemulsions have been advanced in the literature. It has also been found that the form of the employed entropy term may significantly influence the deduced values for the elastic moduli κ and $\bar{\kappa}$ [29,55]. Therefore we want to illuminate how various assumptions for the entropic term may influence the outcome of our discussion, especially since it is exclusively the entropy term that is responsible for the concentration dependence of the microemulsion properties such as equilibrium radius, polydispersity, and interfacial tension. This is now of particular interest since in our dilution experiments (see Sec. IV D) we checked this concentration dependence experimentally in some detail.

We may recall that in general the total energy F of a microemulsion system should be given by the sum of the bending energy F_b and an entropic term $F_{\rm ent}$, as detailed in Eq. (1). The entropy of mixing term to the free energy of the droplet system can in general be written as

$$F_{\rm ent}=NkTf(\Phi) \tag{B1}$$

since it should depend exclusively on the volume fraction [via $f(\Phi)$], as we assume that no other interactions than the steric exclusion should be present between the aggregates. The term $f(\Phi)$ will now depend on certain assumptions regarding the system. In all our evaluations in the main part we used [Eq. (4), case I]

$$f(\Phi)=(1/\Phi)\{\Phi\ln\Phi+(1-\Phi)\ln(1-\Phi)\}\ , \tag{B2}$$

as it arises from a random mixing approximation and has been used by Milner and Safran [25].

However, there exist other possibilities for the entropy term. The simplest assumption would be that of ideal mixing, as has been used before to describe the mixing of microemulsion droplets [27]. In that case the entropy of mixing will be given by

$$\Delta S=Nk(x_1\ln x_1+x_2\ln x_2)\ , \tag{B3a}$$

x_i being the corresponding mole fraction. If we now assign the solvent molecules to be one component of the system, and the microemulsion droplets to be the other component, we may rewrite the entropic contribution as (here, as in the following equations, R is the aggregate radius and V_S the volume of a solvent molecule; case II):

$$f(\Phi)=\ln(\Phi)-\ln(1-\Phi)-3\ln[R\ (\text{Å})] -\ln(4\pi/\{3[V_S\ (\text{Å}^3)]\})-1\ , \tag{B3b}$$

If one further takes into account the hard-sphere repulsion, as it should become increasingly important for higher concentrations, one may use the equation of state as given by Carnahan and Starling [50], and deduce from that the following relation for f (case III) [58]:

$$f(\Phi)=\ln(\Phi)+\Phi\frac{4-3\Phi}{(1-\Phi)^2}-3\ln[R(\text{Å})] -\ln(4\pi/\{3[V_S\ (\text{Å}^3)]\})-1\ . \tag{B4}$$

Finally a different entropy term has also been proposed, which arises upon taking into account the free Brownian displacement in the dispersion medium. This treatment, originally due to Reiss [59], was later applied by Over-

beek *et al.*[60] as well as recently by Kegel, Bodnàr, and Lekkerkerker to droplet microemulsions (case IV, where here V_0 is the volume of the solubilized molecule, in our case the oil):

$$f(\Phi)=\ln(\Phi)+\Phi\frac{4-3\Phi}{(1-\Phi)^2}-4.5\ln[R(\text{Å})] \\ -1.5\ln\{16/[V_0(\text{Å}^3)]\}-1 . \quad \text{(B5)}$$

The various expressions are somewhat similar, insofar as their leading term for low concentrations is always a $\ln\Phi$ term. However, its absolute values will vary significantly, especially for all the expressions that depend on the volume of the solvent molecule V_0. In the case of water one can take its molecular volume, but this may already induce a large error since it is well known that water is all but a simple molecular liquid [61]. It is highly aggregated, thereby significantly reducing the entropy of the individual water molecules, and in reality it would probably be required to insert for V_0 an effective volume of the unities that are present as apparent structural units in the water. However, such an effective volume is difficult to judge, and therefore this uncertainty about its proper value introduces already a fairly large error in Eqs. (B3)–(B5). It might also be mentioned that recent work regarding the entropy term for vesicles yielded an additional term of the $\ln(R)$ type that has an opposite sign to those in Eqs. (B3)–(B5) and that arises from a finite-size contribution to the fluctuation free energy [56]. It seems quite likely that similar terms should also be taken into consideration for microemulsion systems.

Derivation of structural properties and interfacial tension in terms of the elastic constants

In the following we want to study how the use of the different expressions for the entropic contribution to the free energy will influence the outcome for the evaluation of the elastic constants. For this purpose we will consider in detail how one arrives at expressions that relate the elastic constants to experimentally observable parameters, such as particle size, polydispersity, and interfacial tension.

The starting point of all these conditions is the free energy F of a droplet system that should in general be given by Eq. (1). For a system of monodisperse spheres (here this assumption of monodispersity should not significantly influence the outcome of the discussion) F may be calculated in a straightforward manner where the number of particles N is directly related to the total surface A_0 (which for a system of given surfactant concentration should be a constant) by $N=A_0/4\pi r^2=A_0c^2/4\pi$ (with $c_1=c_2=c$). Employing this relation we arrive at the following expression for the free energy:

$$F=2A_0\kappa(c-c_0)^2+A_0\bar{\kappa}c^2+A_0[kT/4\pi]c^2f(\Phi) . \quad \text{(B6)}$$

A microemulsion that is in equilibrium with the excess of solubilized material may now adjust its radius in such a way as to minimize its free energy. Differentiating (B6) with respect to the curvature c leads to

$$\frac{dF}{A_0dc}=4\kappa(c-c_0)+2\bar{\kappa}c+(kT/4\pi)c\left[2f(\Phi)+c\frac{df(\Phi)}{dc}\right] \\ =4\kappa(c-c_0)+2\bar{\kappa}c+(kT/4\pi)c \\ \times\left[f(\Phi)+D+c\frac{dg(\Phi)}{d\Phi}\frac{d\Phi}{dc}\right] . \quad \text{(B7)}$$

One has also to differentiate the entropy term $f(\Phi)$ since the volume fraction Φ also depends on the curvature c of the droplets (as only the total surface remains fixed but the droplets may grow by incorporating the excess phase, thereby at the same time increasing the volume fraction). Here we may split $f(\Phi)$ into a part $g(\Phi)$ that depends explicitly on Φ [compare Eqs. (B3)–(B5)] and D that arises from the $\ln R$ terms in $f(\Phi)$. Therefore $D=0$ for case I, 1.5 for cases II and III, and 2.25 for case IV.

We may now simplify the last term, since for a system of spheres with a constant total surface simple geometry requires that the droplet radius r should scale linearly with the droplet volume fraction Φ_d (for an O-W system, the volume fraction of the oil plus the hydrophobic part of the surfactant that is contained in the droplet) according to

$$r=1/c=3\frac{v_s}{a_s}\frac{\Phi_d}{\Phi_s} . \quad \text{(B8)}$$

Here v_s and a_s are the volume and head group area per surfactant molecule, and Φ_s the volume fraction of the surfactant that is incorporated in the droplets, i.e., for the case of O-W droplets its hydrophobic moiety. If we consider the somewhat more complicated case that the surfactant molecule possesses a fairly large hydrophilic head group (as for instance applies to the nonionic surfactants of the type C_nE_j), we find that the real volume fraction Φ (the volume that is taken up by surfactant plus oil) would be given by the sum of Φ_d plus a constant term Φ_h that accounts for the volume taken up by the hydrophilic heads of the surfactant (in that case one also has to consider that v_s has to be the volume of the hydrophobic part of the surfactant). This then leads directly to a relation between the volume fraction Φ and the curvature c that allows for a simple calculation of $d\Phi/dc$:

$$\Phi=\frac{\Phi_s a_s}{3v_s c}+\Phi_h , \quad \text{(B9a)}$$

$$\frac{d\Phi}{dc}=-\frac{\Phi_s a_s}{3v_s c^2} . \quad \text{(B9b)}$$

Then we may rewrite (B9a) as

$$\frac{\Phi_s}{\Phi}=\frac{3v_s c}{a_s}\left[1+\frac{3v_s c}{a_s}\frac{\Phi_h}{\Phi_s}\right]^{-1}=\frac{3v_s c}{a_s}B . \quad \text{(B9c)}$$

Inserting this term in (B7) leads to [with $g'(\Phi)=dg(\Phi)/d\Phi$]

$$\frac{dF}{A_0 dc} = 4\kappa(c-c_0)+2\bar{\kappa}c+(kT/2\pi) \times c[f(\Phi)+D-\Phi g'(\Phi)B/2] . \quad \text{(B10)}$$

Equating this with zero, we obtain for the minimum curvature c_m, or equivalently for the maximum radius R_m, the following relation:

$$\frac{R_m}{R_0}=\frac{c_0}{c_m}=\frac{2\kappa+\bar{\kappa}+\frac{kT}{4\pi}[f(\Phi)+D-\Phi g'(\Phi)B/2]}{2\kappa} . \quad \text{(B11)}$$

This relation is now insofar different from the one used before [Eq. (3) in the original text] as it also contains the $g'(\Phi)$ term that arises from the fact that the volume fraction itself depends on the radius that is attained by the system under equilibrium conditions. For our four cases $\Phi g'(\Phi)$ is just given by the following:

Case I,

$$-\frac{\ln(1-\Phi)}{\Phi} .$$

Case II,

$$\frac{1}{1-\Phi} .$$

Cases III and IV,

$$\frac{1+\Phi+\Phi^2-\Phi^3}{(1-\Phi)^3} .$$

This modification for the maximum radius R_m attained by the microemulsion droplets also translates, however, into the formula for the polydispersity [Eq. (6c)], since it is obtained by inserting the ratio R_m/R_0 into Eq. (6a). Doing so with the modified expression for R_m leads us directly to

$$4\pi p^2=\langle|u_0|\rangle^2 = \frac{kT}{2(2\kappa+\bar{\kappa})+\frac{kT}{2\pi}[f(\Phi)-2D+\Phi g'(\Phi)B]} . \quad \text{(B12)}$$

Similarly we may modify Eq. (5) that relates the elastic constant to the macroscopically observed interfacial tension, which leads to

$$\gamma R^2=2(2\kappa+\bar{\kappa})+\frac{kT}{4\pi}[f(\Phi)+2D-\Phi g'(\Phi)B] . \quad \text{(B13)}$$

Influence of these corrections for the various entropic terms on the interpretation of our SANS results

Finally we want to look at the quantitative influence of these corrections on the interpretation of our SANS results in terms of the elastic constants. First let us estimate the magnitude of the term that arises from differentiating $f(\Phi)$. For the surfactant system $C_{10}E_4$-decane, the correction factor B may be approximated using for a_s (46.5 Å^2) (as calculated from the SANS results) and v_s (307 Å^3) (obtained by using a density of 0.85 g/ml). With these values, taking $1/c=50$ Å (as the experiments have shown) and assuming that $\Phi_s=\Phi_h$, an assumption that for this surfactant (as well as for the other employed surfactants) should be very realistic, one can calculate B to be 0.71. In Fig. 12 we have plotted $\Phi g'(\Phi)$, and from that it is clear that for cases I and II this term will always be much smaller than 2, which means that the total term $\Phi g'(\Phi)B/2$ will always be less than 0.5 (for volume fractions up to 0.3) which means it is only a fairly minor modification compared to the other factors. This situation is somewhat different for cases III and IV that contain the hard-sphere repulsion term. Here this factor will be significantly larger for the case of high concentration, and lead to some changes for the numerical values of the elastic constants.

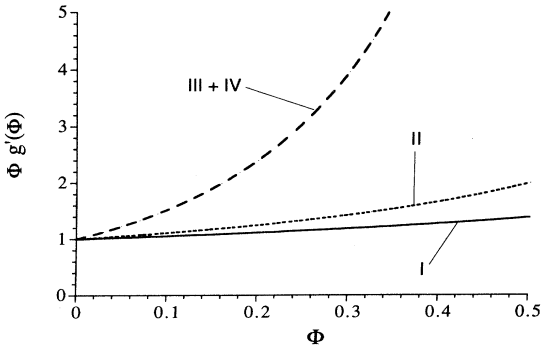

FIG. 12. The term $\Phi g'(\Phi)$ as a function of the volume fraction Φ.

However, for concentrations that are not too high ($\Phi<0.2$), we may state quite generally that the term $\Phi g'(\Phi)B$ should be fairly small (<1), and may in a first approximation well be neglected (as done in the main part of this paper), especially if we consider that it is not larger than the uncertainty that is introduced by having to account for the molecular volume in cases II–IV.

Nonetheless we reanalyzed our dilution series data upon using the four different entropy terms in full detail, as described above. For the molecular volume of the solvent molecules we chose that of a water molecule (30 Å^3). With that, and taking $B=0.71$, we calculated the term that arises from the entropy contribution in Eq. (B11) for

TABLE VI. Values for $(2\kappa+\bar{\kappa})/kT$ as deduced from the concentration dependence of the radii (R) and the polydispersity index (p) for the different assumptions regarding the entropy term.

Quantity	Original	Case I	Case II	Case III	Case IV
R: $(2\kappa+\bar{\kappa})/kT$	2.02	2.03	2.47	2.58	2.68
p: $(2\kappa+\bar{\kappa})/kT$	2.75	2.63	5.79	4.66	5.72

TABLE VII. Values for $(2\kappa+\bar{\kappa})/kT$ for the different cases for the samples with different chain length of the surfactant. The values were derived via two routes: the polydispersity index [marked (p)] and the interfacial tension [marked (γ,R)].

Surfactant	Original	Case I	Case II	Case III	Case IV
C_8E_3; (p)	1.20	1.14	2.17	2.13	2.53
C_8E_3; (γ,R)	0.90	1.05	1.61	1.61	1.77
$C_{10}E_4$; (p)	2.28	2.22	3.24	3.20	3.58
$C_{10}E_4$; (γ,R)	2.34	2.40	2.94	2.93	3.08
$C_{12}E_5$; (p)	3.42	3.36	4.37	4.33	4.71
$C_{12}E_5$; (γ,R)	3.50	3.55	4.08	4.08	4.22

TABLE VIII. Values for $(2\kappa+\bar{\kappa})/kT$ for the different cases for the samples with different chain lengths of the hydrocarbon. The values were derived via two routes: the polydispersity index [marked (p)] and the interfacial tension [marked (γ,R)].

Oil	Original	Case I	Case II	Case III	Case IV
decane; (p)	2.28	2.22	3.24	3.20	3.58
decane; (γ,R)	2.34	2.40	2.94	2.93	3.08
octane; (p)	2.32	2.26	3.34	3.30	3.72
octane; (γ,R)	2.75	2.81	3.42	3.41	3.59
heptane; (p)	2.30	2.24	3.34	3.30	3.73
heptane; (γ,R)	2.26	2.32	2.96	2.95	3.11
hexane; (p)	2.27	2.21	3.36	3.30	3.76
hexane; (γ,R)	1.97	2.03	2.71	2.70	2.91

the individual cases, and fitted our experimental data for the radii to this linear expression (since in principle one may rewrite (B11) as $R_m=a(2\kappa+\bar{\kappa})+b[f(\Phi)+D-\Phi g'(\Phi)B/2]$). Doing so yields about the same quality of fits for all cases, and the obtained values for $2\kappa+\bar{\kappa}$ (marked R) are given in Table VI together with the original value obtained via Eqs. (3) and (4). The correction introduced by differentiating for the curvature dependence of the volume fraction has hardly any influence at all (compare values for the original and case I). For cases II–IV the values are larger by about 25%, which would still be in reasonable agreement.

In a next step, for the different models we also evaluated the dependence of the polydispersity according to Eq. (B13) as described in the main part of the paper. The obtained values for $2\kappa+\bar{\kappa}$ (marked p) are also given in Table VII. Again the consideration of the $\Phi g'(\Phi)B$ term does not significantly change the outcome for $2\kappa+\bar{\kappa}$, but we find markedly higher values for the cases II–IV. This leads us to the conclusion that our originally employed expression for the entropy of mixing seems to be quite justified since it describes fairly self-consistently both the volume dependence of the radii and the polydispersity index. For the other three entropy models a discrepancy arises of a factor of 2, much too large to be explained by experimental errors. Judging from that the procedure employed in the main part of the paper to deduce the elastic constants from the experimentally observed quantities appears to be quite reliable. Here it might also be added that the problem that arose in Sec. IV D, i.e., that the polydispersity changes much more than predicted by theory, remains valid for all four cases, i.e., the prefactor of the concentration dependent term is always about 2–3 times larger than according to (B12).

Finally for the various cases we recalculated the value that one obtains for $2\kappa+\bar{\kappa}$ for the samples contained in Tables I and V. For all cases it is evident that consideration of the term arising from the differentiation of the volume-fraction-dependent term leads only to marginal changes for case I (that we employed in the main part of the paper). In contrast, the use of the other expressions for the entropic contribution leads in all cases to significantly higher values. For the $C_{10}E_4$-decane system it is also significantly larger than that obtained above from analyzing the concentration dependence of R. Evidently cases II–IV do not yield a self-consistent picture for our experimental data.

Judging from the comparison of the application of the different expressions for the entropic term to our experimental data, we may state that case I, as it was employed in the main part of the paper, seems to be by far the most suitable choice since it allows for a self-consistent interpretation of all our data. In addition it yields the lowest value for the sum $2\kappa+\bar{\kappa}$, and comparison with data from ellipsometry [29] for κ indicates that a lower value seems to more realistic. Finally it might be remarked that the larger change of the polydispersity than what was predicted by theory remains for all tested entropy terms, and seems to have a reason beyond the choice of a particular expression for the entropy of mixing term.

[1] L. M. Prince, *Microemulsions: Theory and Practice* (Academic, New York, 1977).
[2] *Microemulsions,* edited by I. D. Robb (Plenum, New York, 1982).
[3] D. Langevin, Mol. Cryst. Liq. Cryst. **138**, 259 (1986).
[4] L. E. Scriven, Nature **263**, 123 (1976).
[5] Y. Chevalier and T. Zemb, Rep. Prog. Phys. **53**, 279 (1990).
[6] D. Langevin, Annu. Rev. Phys. Chem. **43**, 341 (1992).
[7] W. Helfrich, Z. Naturforsch. **28**, 693 (1973).
[8] P. G. de Gennes and C. Taupin, J. Phys. Chem. **86**, 2294 (1982).
[9] S. Mukherjee, C. A. Miller, and T. Fort, Jr., J. Colloid Interf. Sci. **91**, 223 (1983).
[10] S. A. Safran and L. E. Turkevich, Phys. Rev. Lett. **50**, 1930 (1983).
[11] D. Andelman, M. E. Cates, D. Roux, and S. A. Safran, J. Chem. Phys. **87**, 7229 (1987).

[12] D. Langevin, Adv. Colloid Interf. Sci. **34**, 583 (1991).
[13] L. T. Lee, D. Langevin, and R. Strey, Physica A **168**, 210 (1990).
[14] E. van der Linden, S. Geiger, and D. Bedeaux, Physica A **156**, 130 (1989).
[15] B. P. Binks, J. Meunier, O. Abillon, and D. Langevin, Langmuir **5**, 415 (1989).
[16] M. Borkovec and H. F. Eicke, Chem. Phys. Lett. **157**, 457 (1989).
[17] M. Kummrow and W. Helfrich, Phys. Rev. A **44**, 8356 (1991).
[18] K. Shinoda and S. Friberg, Adv. Colloid Interf. Sci. **4**, 281 (1975).
[19] M. Kahlweit and R. Strey, Angew. Chem. Int. Ed. **24**, 654 (1985).
[20] D. Anderson, H. Wennerström, and U. Olsson, J. Phys. Chem. **93**, 4243 (1989).
[21] H. Kunieda and K. Shinoda, J. Dispers. Sci. Tech. **3**, 233 (1982).
[22] M. Kahlweit, R. Strey, and P. Firman, J. Phys. Chem. **90**, 671 (1986).
[23] S. A. Safran, J. Chem. Phys. **78**, 2073 (1983).
[24] S. A. Safran, in *Structure and Dynamics of Strongly Interacting Colloids and Supramolecular Aggregates in Solution,* Vol. 369 of *NATO Advanced Study Institute, Series C: Mathematical and Physical Sciences,* edited by S. H. Chen, J. S. Huang, P. Tartaglia (Kluwer, Dordrecht, 1992).
[25] S. T. Milner, S. A. Safran, Phys. Rev. A **36**, 4371 (1987).
[26] S. A. Safran, Phys. Rev. A **43**, 2903 (1991).
[27] M. Borkovec, J. Chem. Phys. **91**, 6268 (1989).
[28] M. Borkovec, Adv. Colloid Interf. Sci. **37**, 195 (1992).
[29] F. Sicoli, D. Langevin, and L. T. Lee, J. Chem. Phys. **99**, 4759 (1993).
[30] J. P. Cotton in *Neutron, X-ray and Light Scattering,* edited by P. Lindner and T. Zemb (Elsevier, New York, 1991), p. 19.
[31] *Light Scattering by Liquid Surfaces and Complementary Techniques,* edited by D. Langevin, Surfactant Science Series Vol. 41 (Marcel Dekker, New York, 1992).
[32] J. E. Bowcott and J. H. Schulman, Z. Elektrochem. **59**, 283 (1955).
[33] W. Stoeckenius, J. H. Schulman, and L. M. Prince, Kolloid-Z. **169**, 170 (1960).
[34] J. Meunier and L. T. Lee, Langmuir **7**, 1855 (1991).
[35] J. S. Huang, S. T. Milner, B. Farago, and D. Richter, Phys. Rev. Lett. **59**, 2600 (1987).
[36] B. Farago, D. Richter, J. S. Huang, S. A. Safran, and S. T. Milner, Phys. Rev. Lett. **65**, 3348 (1990).
[37] A. Guinier and G. Fournet, *Small-Angle Scattering of X-rays* (Wiley, New York, 1955).
[38] B. Zimm, J. Chem. Phys. **16**, 1093 (1948).
[39] N. W. Ashcroft and J. Lekner, Phys. Rev. **145**, 83 (1966).
[40] J. Skov Pedersen, D. Posselt, and K. Mortensen, J. Appl. Crystallogr. **23**, 321 (1990).
[41] M. Gradzielski, D. Langevin, L. Magid, and R. Strey, J. Phys. Chem. **99**, 13 232 (1995).
[42] J. R. Lu, Z. X. Li, T. J. Su, R. K. Thomas, and J. Penfold, Langmuir **9**, 2408 (1993).
[43] P. D. Fletcher and R. Johannsson, J. Chem. Soc. Faraday Trans. **90**, 3567 (1994).
[44] M. J. Rosen, A. W. Cohen, M. Dahanayake, and X.-Y. Hua, J. Phys. Chem. **86**, 541 (1982).
[45] I. Szleifer, D. Kramer, A. Ben-Shaul, D. Roux, and W. Gelbart, Phys. Rev. Lett. **60**, 1966 (1988).
[46] C. R. Safinya, E. B. Sirota, D. Roux, and G. S. Smith, Phys. Rev. Lett. **62**, 1134 (1989).
[47] M. Teubner, J. Chem. Phys. **95**, 5072 (1991).
[48] V. F. Sears, AECL-8490, Chalk River Nuclear Laboratory, 1984.
[49] L. Cser, B. Farago, T. Grosz, G. Jancso, and Yu. M. Ostanevich, Physica B **180&181**, 848 (1992).
[50] N. F. Carnahan and K. E. Starling, J. Chem. Phys. **51**, 635 (1969).
[51] G. Oetter and H. Hoffmann, Colloid Surf. **38**, 225 (1989).
[52] B. P. Binks, H. Kellay, and J. Meunier, Europhys. Lett. **16**, 53 (1991).
[53] M. J. Hou, M. Kim, and D. O. Shah, J. Colloid Interf. Sci. **123**, 398 (1988).
[54] R. A. Hudson and B. A. Pethica, in *Chemistry and Physics of Applied Surface Active Substances, Proceedings of the 4th International Congress, 1964,* edited by J. Th. B. Overbeck (Gordon & Breach, New York, 1964), Vol. 4, p. 631.
[55] W. K. Kegel, I. Bodnàr, and H. N. W. Lekkerkerker, J. Phys. Chem. **99**, 3272 (1995).
[56] D. C. Morse and S. T. Milner, Europhys. Lett. **26**, 565 (1994).
[57] B. Cabane, R. Duplessix, and T. Zemb, in *Surfactants in Solution,* edited by K. L. Mittal and B. Lindman (Plenum, New York, 1984), Vol. 1, p. 373.
[58] J. Th. G. Overbeek, Faraday Discuss. Chem. Soc. **65**, 7 (1978).
[59] H. Reiss, J. Colloid Interf. Sci. **53**, 61 (1975).
[60] J. Th. G. Overbeek, G. J. Verhoeckx, P. L. de Bruyn, and H. N. W. Lekkerkerker, J. Colloid Interf. Sci. **119**, 422 (1987).
[61] H. S. Frank and W. Y. Wen, Discuss Faraday Soc. **24**, 133 (1957).